POLITECNICO DI TORINO

Department of Mechanical and Aerospace Engineering (DIMEAS)

Master's degree in biomedical engineering

Exploiting ligand multivalency to selectively target HER2 receptor in glioblastoma

Lab supervisors:
Giuseppe Battaglia
Matilde Ghibaudi

Relators:
Gianluca Ciardelli
Clara Mattu
Claudia Di Guglielmo

Candidate:
Elisa Mastrantuono

Academic year 2022/2023

Abstract

Glioblastoma (GBM) is the most common and fatal primary malignant tumor in the central nervous system (CNS). The main genetic alterations involved in GBM regard the PI3K/Atk and the MAPK pathways, which can be activated by the epidermal growth factor receptors (HER), and regulate cell cycle and apoptosis. Indeed, HER receptors overexpression in cancer is a poor prognostic marker and, therefore, is becoming a promising therapeutic target. However, the main obstacles to the delivery of drugs into the brain are the tumor microenvironment and the blood-brain barrier, which make selective targeting not trivial to achieve. In this scenario, polymeric nanoparticles functionalized with selective ligands are emerging as powerful vectors to reach into one of the most difficult organs in the human body.

In the present study, we focus on HER2 receptor as a target for drug delivery. Its dimerization with other ligand-bound HER family receptors causes the activation of PI3K and MAPK signaling cascades, leading to uncontrolled growth of cancer cells.

The first aim of this work is to investigate the expression of HER2 receptor on primary GBM cells. Then, we try to identify the optimal number of ligands (KCCYSL peptide) against the HER2 receptor and tethered on spherical polymeric nanoparticles. Here we analyse how the ligand multivalency influences the interaction between the nanoparticles and GBM cells, the ability of the ligand to bind HER2, and the effect on the receptor's biological activity.

Contents

List of Figures

1. Introduction

1.1 Glioblastoma

1.1.1 Clinical problem

Gliomas are defined as tumors originating in the glial cells that support neurons in the brain, including astrocytes, oligodendrocyte, and ependymal cells, and comprehend approximately 85% of all CNS malignant tumors[8]. The most common and aggressive form is glioblastoma multiforme (GBM), which accounts for around 59.2% of gliomas, and is classified as World Health Organization (WHO) grade IV[8].

GBMs can be classified into two main classes, identified as primary and secondary GBM. Primary lesions occur without previous evidence of a less-malignant precursor and represent the majority of cases in older patient. On the other hand, secondary lesions derive from lower grade atrocytomas that progress into GBMs. These cases are quite rare and tend to occur in younger patients[9]. Despite differences in the genetic alterations involved, both GBM subtypes present the same pathological and phenotypical features. In fact, the genetic alterations implicated in both the subtypes regard pathways that control cell proliferation and cell survival, such as the phosphoinositide 3'-kinase (PI3K) and the mitogen-activated protein kinase (MAPK), causing uncontrolled cell growth and high immune resistance. Other important hallmarks of GBM are the rapid infiltration in the surrounding tissues, and the dramatic increase in microvasculature proliferation through angiogenesis processes[9].

At a phenotypical level, both primary and secondary GBM present as heterogeneously enhancing masses with surrounding edema, and a central necrotic area. The intrinsic heterogeneity is due to the presence of intratumoral cellular niches with different phenotypic characteristics, that are maintained by interactions with the tumor microenvironment. These interactions are due to the activation of several pathways that leads to the recruitment of endothelial cells, astrocytes, and microglia to the tumor, causing what is called extrinsic heterogeneity[10,11]. The tumor mass is characterized by

a central area that consists of necrotic tissue, representing almost 80% of the tumor, and by highly proliferating cancer cells in the peripheral zone[9]. These cancer stem cells contribute to resistance of GBM to standard treatments, leading to an high degree of morbidity and mortality of patients and to a very poor prognosis. It has been estimated that only 5% of patient survive after 5 years from the diagnosis[12], while the median survival has remained at 12 months over the past decade[9].

1.1.2 Clinical presentation and diagnosis

It is not possible to identify a typical clinical presentation of GBM, mainly due to the fact that possible symptoms can vary depending on the size and the location of the tumor, and on the anatomic structures involved in the brain[13]. Typically the first clinical sings are those caused to the increased intracranial pressure, such as headaches, vomiting, and focal or neurological deficits. Also epileptic seizure can be seen as a recurrent GBM symptom[12].

The initial diagnosis usually include computed tomography (CT) or magnetic resonance imaging (MRI) scan of the brain, leading to the detection of heterogeneously enhancing mass with surrounding edema, suggesting the presence of a malignant glioma. Through an histopathological examination of a part or the entire mass of the tumor is possible to have a definitive diagnosis, based on traditional histological, cytologic and histochemical methods[14].

1.1.3 Therapeutic approaches

The standard therapeutic approach for newly diagnosed GBM consists in surgical resection, followed by radiotherapy with concomitant and adjuvant chemotherapy with temozolomide (TMZ). Complete surgical resection is not possible because of the high infiltrating nature of GBMs and its extensive vascularization. However, the removal of great part of the tumor, whenever possible, can provide tissues for histological analysis and reduce the symptoms due to the mass effect, facilitating adjuvant therapies. The addition of radiotherapy, and concomitant chemotherapy to surgery can increase survival among patients, from 3-4 months to 14 months[15]. Therefore, the current standard therapies improved median survival but the disease remains basically incurable, due to the late stage of the disease at diagnosis, and the inability of available therapy to efficiently eradicate all GBM cells. As a result, nearly all cases of GBM eventually recur, with a median time-to-progression of 6.9 months. Surgical intervention may provide symptomatic relief from mass effect, but it confers no significant survival benefit. Similarly,

radiotherapy and chemotherapy exhibit limited efficacy in the management of recurrent GBM, leading to a median survival of approximately 5-7 months[16].

Thus, there is the urgent need for the development of advanced therapies for GBM that not only improve patient survival but also minimize the side effects of current medical treatments. In the past decade, new discoveries have been made, and a more extensive knowledge in GBM biology and genetic is now available. Large efforts have been invested in comprehending the genetic abnormalities in signaling pathways that trigger tumor growth and invasiveness. Exploiting this knowledge , it is now possible to investigate and design individualized targeted therapies for glioma treatment[17,18].

1.1.4 Targeted therapies

The aim of numerous recent investigations is to develop innovative therapies that selectively target molecules that are either overexpressed or mutated in malignant cells. These molecules cause the activation of signaling pathways, leading to the specific cancer hallmark analyzed in **Section 1.1.1**. Targeting them can increase treatment's specificity and mitigate toxicity induced by delivery to non-malignant cells. This is extremely important because the side effects associated with standard therapies limit the dose that can be administrated to the patient, leading to tumor progression and to drug-resistance development[19]. The target molecule selected must exhibit effective and highly specific targeting properties to facilitate selective treatment, and also exhibit high expression levels in the tumor region are needed in order to enable a stable interaction. However, if the expression is identical in healthy cells, the likelihood of developing toxicity and side effects increases.

The most common type of targeted therapy in all types of cancer is directed against alterations that cause an aberrant activation of growth factor receptor tyrosine kinases (RTKs). Also in the case of GBM, alterations in RTKs and downstream MAPK/PI3K represent an important hallmark, and then a possible target[20].

One of the main activator of these pathways in cancer is represented by the human epidermal growth factor receptors family.

1.2 Human epidermal growth factor receptors

Human epidermal growth factor receptors (HER/ErbB) are a family composed of four transmembrane receptors with protein-tyrosine kinase activity, illustrated in **Figure 1.1**. Protein kinase signaling has a crucial role in cell biology. These receptors are involved

in cell proliferation, division, mitosis and other important activities for the cell physiological functions, and any malfunction in their activity can result in various diseases, including cancer[1].

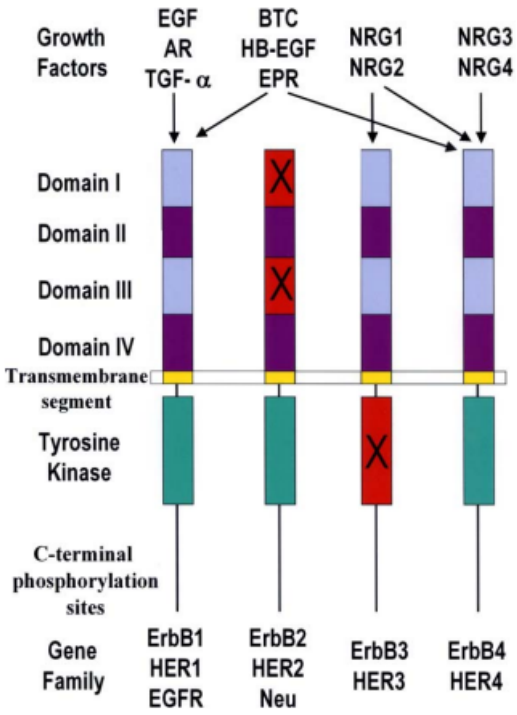

Figure 1.1: ErbB gene family and EGF family of ligands. Those denoted with an X are the inactive domains, ligand-binding domain in the case of ErbB2 and kinase domain in case of ErbB3[1].

The common structure of ErbB receptors consists of a cystein-rich extracellular ligand binding domain (ECD), a single alpha-helix transmembrane lipophilic domain, and a cytoplasmatic domain with tyrosine kinase catalytic activity[21]. Their activation depends on ligand-incited dimerization. HER1 is activated by different ligands, e.g. EGF, transforming growth factor α (TGFα), amphiregulin and epiregulin, HER3 and HER4 are both activated by neuregulins (NGFs), while there is no ligand known to bind HER2 receptor[21].

In normal conditions, the ECD domain of HER receptors is presented in the closed configuration, with the dimerization arm hidden in the structure, maintaining the receptor in an auto-inhibiting form. Upon ligand-biding, a substantial domain rearrangement causes the switch between the inactive and the active conformation of the receptor. This

rearrangement gives rise to the extended conformation allowing the dimerization arm to participate in intramolecular interaction, and so allowing heterodimerization or homodimerization with other receptors. Dimer formation happens because the complex of two receptors and a ligand presents higher stability compared to the single receptor [1,21]. The dimerization induces the activation of the cytoplasmatic kinase, which in turn leads to autophosphorylation of the tyrosine and initiation of downstream signaling events. Therefore, HER network consists of an input layer, the ligands, an information processing layer, the receptor, and an output layer characterized by cell growth, differentiation or migration. Receptor dimerization is fundamental to activate signaling network [21].

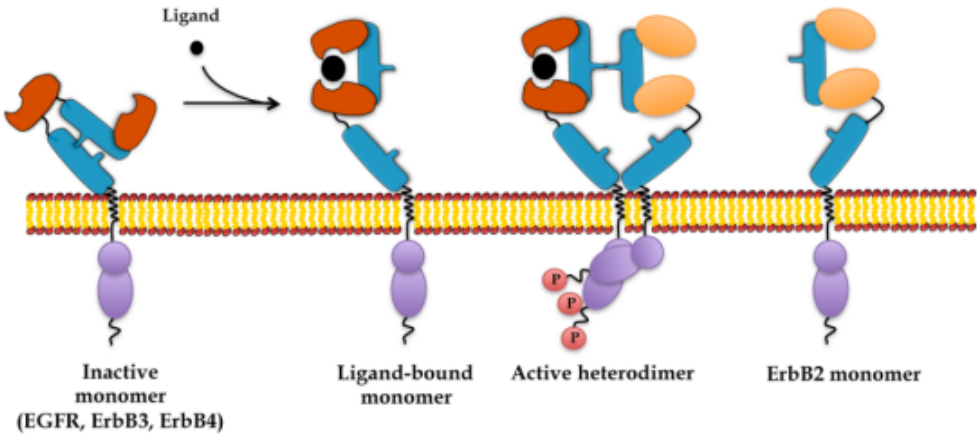

Figure 1.2: HER receptor dimerization and activation. In HER1, HER3, and HER4 receptors, ligand-binding allows the receptor homo- and heterodimerization which causes the activation of signaling pathways. HER2 is represented in his fixed open conformation, ready to interact with other HER receptors [2].

In this scenario, HER2 receptor can adopt a fixed open conformation resembling a ligand activated state, but allowing it to dimerize also in the absence of a specific ligand. This particular conformation enables HER2 to act as a co-receptor for multiple ligands, facilitating the formation of heterodimers with all other members of its receptor family. In the context of cancer, where HER2 is often overexpressed, it can also form homodimers [2]. HER dimerization and activation is summarized in **Figure 1.2**.

Heterodimers generate more potent signals compared to homodimers, and HER2 represents the preferred partner in heterodimer formation, leading to the most potent signaling pathways. HER2 is a slowly internalizing receptor and it is characterized by a slow ligand dissociation, thus, signaling activated by HER2-containing dimers is

relatively prolonged[21].

1.2.1 The role of HER2 receptor in cancer

HER2 is a 1255 amminoacids, 185 kD transmembrane glycoprotein, and its structure is showed in **Figure 1.3**.

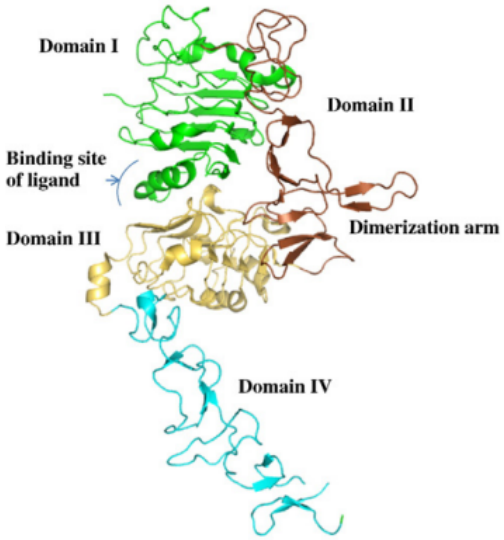

Figure 1.3: HER2 structure: the N-terminal ECD contains approximately 600 residues, which could be divided in four subdomains (I-IV). Subdomains I and III represents the possible binding sites for potential ligands, while subdomains II and IV are involved in homo- and heterodimerization[3].

In normal conditions it has a fundamental role in activating and governing a rich network of signaling pathways that control normal cell growth, differentiation, motility, and adhesion. But a dysregulation of this network has been observed in cancer cells, where an excessive expression of HER2 receptor caused a growth advantage[22]. Overexpression of this receptor can in fact trigger different mechanisms leading to excessive cell proliferation and survival.

An high availability of HER2 receptors leads to an aberrant homo- and heterodimers formation and so to an excessive signaling. Moreover, HER2 makes ligand-receptor interaction stronger, due to its slow ligand dissociation rate and it weakens other receptor specificity. Also the process of internalization and degradation could be blocked in case of HER2-containing dimers[23]. Therefore, all these mechanisms, enhancing and

prolonging signals that trigger cell transformation, have a causal role in the promotion of carcinogenesis. As a consequence, cancers presenting the amplification of ErbB2 gene are an aggressive form, resistant to chemotherapy, and characterized by an increased mortality rate[23].

1.2.1.1 Principal pathways

After dimerization, the cross-phosphorylation leads to the formation of docking sites for the engagement of downstream signaling elements. Different ligands and receptors recruited by HER2 can lead to different intracellular signaling cascades. For example, HER2-HER3 heterodimer is known to have the most active signaling complex amond tyrosine kinase dimers, and it triggers the induction of PI3K lipid kinase activity, while all the others HER2 involved dimerization can activate the MAPK pathway. These two pathways, associated with cell proliferation and apoptosis arrest[3], are summarized in **Figure 1.4**.

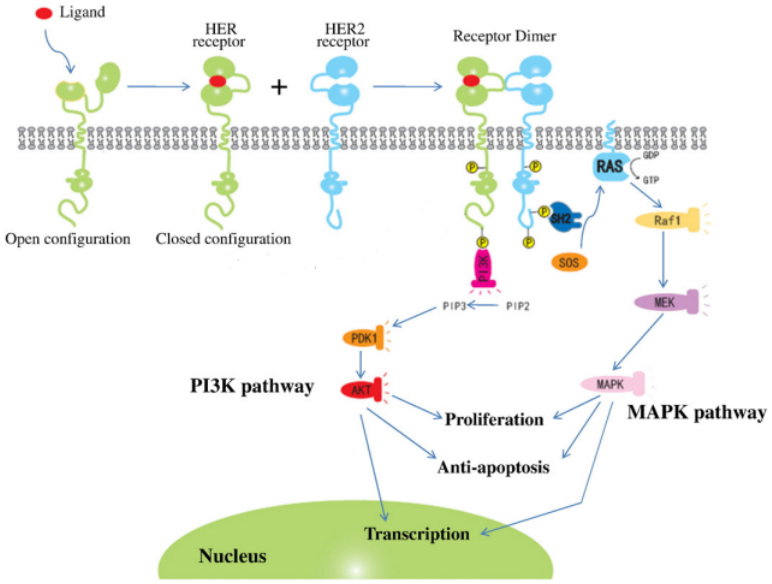

Figure 1.4: Main oncogenic pathways activated by HER2: receptor activation leads to the phosphorylation of intracellular tyrosine residues and the initiation of downstream transduction pathways with oncogenic consequences[3].

Phosphoinositide 3-kinase (PI3K/Akt) pathway

PI3K pathway is initiated by the binding of growth factors to the tyrosine kinase receptor HER3, leading to the dimerization with HER2. Then, the lipid kinase PI3K is recruited to the internal docking site where it interacts with the phosphorylated serine or threonine residues of the receptor, becoming activated. The activated PI3K converts PIP2 [phosphatidylinositol (3,4)-bisphosphate] into its active form, PIP3 [phosphatidylinositol (3,4,5)-trisphosphate]. Following that, PIP3 adds a phosphate group to Akt (protein kinase B), which then binds to various transcription factors that regulate cell cycle progression, inhibit programmed cell death, and promote cell survival. PI3K/Atk pathway has a natural inhibitor, PTEN (phosphatase and tensin homolog), whose function is to dephosphorylate PIP3, blocking the activation of Atk.

Dysregulation of this pathway has an important role in development of malignancy. Most common alterations include PI3K mutation, which causes an upregulation of the downstream signaling, leading to increased cellular proliferation, and the inactivation of PTEN tumor suppressor gene[24,25].

Mitogen-activated protein kinases (MAPK) pathway

MAPK is initiated by the binding of growth factors to the tyrosine kinase receptors HER1 and HER4 leading to the dimerization with HER2. The interaction between the phosphorylated tyrosine residues and HER2 intracellular domain causes an activation cascade involving Shc (Scr-Homology-2 containing), Grb-2 (growth factor receptor-bound protein 2), Sos (son of sevenless, guanine nucleotide exchange factor) and RAS (rat sarcoma protein). The phosphorylation of RAS kinase triggers the activation of the MAPK signaling pathway, which involves the phosphorylation of Raf, MEK (mitogen-activated protein kinase kinase) and ERK (extracellular signal-regulated kinase) proteins, resulting in ERK translocation to the nucleus. This causes the activation of several transcription factors that mediate gene expression, regulating cell cycle, cell proliferation and apoptosis[24].

An hyperactivation of MAPK pathway results in an aberrant transcription of genes regulating proliferation and migration, thus giving the tumor cells poor differentiation, invasivness and metastatic behavior[26].

1.2.2 HER2 based therapies

The important difference in expression levels between normal cells and HER2-overexpressing cancer cells, together with its important role in cancer progression, makes this receptor

an ideal target for eventual new therapeutic approaches. The most common strategies investigated in the last years include[23]:

- **Small molecules tyrosine kinase inhibitor**. The aim of these treatments is to block the signaling cascades that lead to cancer progression, acting at intracellular level. Lapatinib is a dual protein kinase inhibitor that targets the ATP-binding site of HER2 and the epidermal growth factor receptor (EGFR), preventing self-phosphorylation and so the activation of signaling mechanisms. The results from a phase III clinical trial demonstrated an improvement in median progression-free survival, and a reduced risk of disease progression, in patients treated with lapatinib in combination with other treatments[26,27].

- **Antibody-drug conjugates (ADCs)**. The cytotoxic agent is linked to the antibody (trastuzumab) through a thioether link. This is done in order to overcome antibody resistance by exploiting it to target the cytotoxic agent to HER2 over-expressing cells. Some studies revealed a significantly prolonged progression-free survival and overall survival, with less toxicity compared to tyrosine kinase inhibitors[27].

- **Tumor targeting peptides (TTPs)**. TTPs are becoming an important field in tumor targeted therapies. Compared to ADCs, peptides present better tissue penetration properties, are easy to synthesize and have a high receptor recognition rate and low molecular weight. They could be used as imaging agents or as drug delivery systems if conjugated with a cytotoxic agent[23].

- **Humanized monoclonal antibodies**. Antibodies targeting the ECD of HER2 receptors, preventing homo- and heterodimerization and inducing antibody-dependent cellular toxicity[23]. The first US Food and Drug Administration (FDA) approved monoclonal antibody for cancer treatment was trastuzumab, also known as Herceptin (see **Section 1.2.2.1**).

1.2.2.1 Trastuzumab - Herceptin

Currently, the most common strategies to target HER2 include the use of monoclonal antibodies. The first FDA-approved HER2 targeted therapy was trastumazumab (or Herceptin), used mainly for HER2+ breast cancers. Trastuzumab (TZ) is a humanized monoclonal antibody developed starting from a murine antibody, with two antigen-binding sites that recognize HER2 receptor. It acts through four main mechanisms of

action: (1) it blocks the downstream activity of HER2, causing cell cycle arrest and angiogenesis, (2) it downregulates HER2 receptor, by promoting the action of tyrosine kinase-ubiquitin ligase c-Cbl which in turn leads to HER2 internalization and degradation, (3) it activates the immunological response mediated by the antibody-dependent cellular cytotoxicity (ADCC): the presence of the antibodies leads to the recruitment of natural killer (NK) cells and their activation. However (4) the most well known action is the inhibition of the MAPK and PI3K/Atk pathways. TZ interferes with the dimerization of HER2 by inhibiting its activation and then the deriving signaling cascades. A significant improvement in overall survival have been observed by the use of Herceptin in clinics[24,28].

Despite its significant advancement in cancer therapy, Herceptin's effectiveness is limited in terms of response duration due to the presence of resistance mechanisms, and its low selectivity results in numerous unwanted effects. In fact, even if there is an evident effect on HER2 overexpressing cancer cells, the presence of HER2 receptors in healthy cells causes important side effects like infections, cardiotoxicity and severe lungs diseases[28]. This happens because with monovalent targeting it is not possible to distinguish between surfaces with high and low receptor coverage. It becomes then fundamental the investigation of more selective therapies.

1.3 Super selective targeting

Paul Ehrlich's "magic bullet" theory, developed over 100 years ago, proposed that chemotherapy could selectively target disease-causing cells by directing drugs to molecular targets exclusively expressed by cancer cells. This would allow the drugs to kill malignant cells leaving healthy cells unaffected[33]. This theory has inspired extensive research on identifying the right molecules for cancer treatment. In the context of brain cancer, drug delivery systems must be able to cross the blood-brain barrier (BBB) and reach the site of interest, in this case, GBM cells. This is typically achieved by exploiting a ligand present on the surface of nanoparticles (NPs) that can bind to a receptor on the targeted cells. However, targeted drug delivery systems often lack selectivity because the targeted receptor is also present in healthy cells. Many anti-cancer drugs are based on high-affinity monovalent interactions between the cell-binding agent and the target. One classical example is the use of monoclonal antibodies (see **Section 1.2.2.1**) whose lack of selectivity can result in off-target effects and unwanted side effects. This issue highlights the need for more selective targeting strategies in cancer treatment[33].

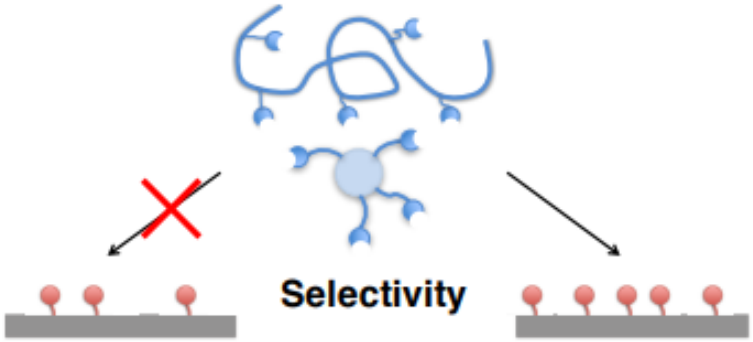

Figure 1.5: Representation of the concept of selectivity: the ability of the system to discriminate between high and low receptor coverage on the cell surface[4].

Multivalency can be employed as a strategy to overcome the problem of low selectivity (see **Figure 1.5**). By using multivalent NPs with more than one ligand, it is possible to create multiple bonds with the substrate (the cell), resulting in a more sensitive and non-linear behavior. Indeed, strong interactions can be generated even if the individual bonds are weak. The probability to separate two entities linked by k bonds can be defined as:

$$p_k^{unbound} \sim (p_1^{unbound})^k$$

Where $p_1^{unbound}$ is the probability that a single bond is broken, and $p_k^{unbound}$ is the probability that all k bonds are broken simultaneously. Given the assumption that the breaking of one bond does not affect the probability of other bonds breaking[4].

In 2017, Curk et al. defined "super-selectivity" as the high sensitivity of the strength of multivalent binding to the number of accessible binding sites on the target surface. The binding of a multivalent NP is then strictly dependent on the concentration of receptors on the cell surface and the number of ligands tethered to the NP[4]. The key challenge is to design ligand-coated NPs that exhibit an "on-off" binding behavior ideal for selective targeting, achieving an almost step-like switch from unbound to bound state as the receptor concentration surpasses a clearly defined threshold value. The phenomenon of switch-like behavior is frequently observed in biological systems, where multivalency is employed to facilitate strong binding, particularly in cases where the univalent interaction between a ligand and receptor is weak. Many bacterial and plant toxins utilize multivalency to achieve impressive selectivity for their target molecules. Similarly, enzymes exploit multivalency to enhance their selectivity by enabling them to simultaneously bind multiple copies of their substrate or a related molecule. Additionally,

many essential biological processes, such as signal transduction and gene expression, depend on selective protein-protein interactions. Therefore, multivalency can enhance this selectivity by enabling a protein to interact with multiple copies of its binding partner simultaneously[4,33,34].

1.3.1 Model

We focus on multivalent nanoparticles that can bind to a receptor-decorated surface. We assume this surface much larger than the NPs, and the NPs larger than the receptors allowing a single NP to bind more receptors simultaneously. In these conditions, the system is regulated by the Langimur isotherm, that defines the fraction of the surface that is occupied by the NPs:

$$\theta = \frac{\rho K_A^{av}}{1 + \rho K_A^{av}}$$

Where ρ is the molar concentration of multivalent NPs in solution, and K_A^{av} is the equilibrium avidity association constant[4]. It is important now to distinguish between the concept of affinity (K_A) and avidity (K_A^{av}). The strength of the interaction between a specific ligand L and its receptor R is quantified by the affinity, which follows the same thermodynamic principles governing reversible reactions.

$$K_A = \frac{k_{on}}{k_{off}}$$

Where k_{on} is rate of binding and k_{off} is the rate of unbinding[35]. Greater ligand affinity enables the receptor to become saturated by a smaller concentration of ligand. High affinity also means that a significant portion of that ligand will bind to any cell that expresses the targeted receptor, rather than exclusively binding to cells that overexpress it. This leads to the problem of low selectivity, causing unwanted interactions and side effects. When considering multivalent systems, it is crucial to include other relevant terms. In such situations, the binding is defined by the avidity, which describes the overall strength of the interaction between a multivalent ligand and its target receptor, and can be defined as the sum of the individual affinities of each ligand-receptor interaction within the system. Therefore, the overall avidity of a multivalent system can be higher than the sum of the affinities of its individual ligands, due to the synergistic effect of multiple binding interactions[35], determined by the individual bond affinities (K_A), the valency of the ligand (k) and the number of the receptor (nR)[4]. The avidity constant incorporates all possible bound states of the multivalent ligand and receptor, including monovalent, bivalent, trivalent, and so on. Representing the sum of the strengths of all

these interactions, the avidity could be written as:

$$K_A^{av} = \Omega_1 K_A + \Omega_2 K_A K_{intra} + \Omega_3 K_A K_{intra}^2 + \dots$$

The first term considers every possible state with a single bond, the second term all doubly bound state, the third all the triply bound, etc. K_{intra} is a constant that determines the internal equilibrium between the singly and doubly bonded states within a system[4]. Ω_i denotes a degeneracy pre-factor, which is also referred to as combinatorial entropy. This type of entropy is exclusive to multivalent interactions and quantifies the number of possible ways in which two multivalent entities can form i bonds. The combinatorial or avidity entropy is invariably positive and promotes the association between a multivalent ligand and a multivalent receptor[5,34,35]. One example of how combinatorial entropy can interfere with multivalent interactions allowing super selectivity is showed in **Figure 1.6**, where Ω is calculated as[4]:

$$\Omega_i = \frac{n_R! k!}{(n_R - i)!(k - i)! i!}$$

In 2011, Martinez-Veracoechea and Frenkel defined selectivity with a parameter α:

$$\alpha = \frac{d\ln\theta}{d\ln n_R}$$

In case of non selective adsorption, this value varies slowly with the increasing of receptors on the surface, never exceeding one. On the other hand, a highly selective system presents a non monotonic behavior, with a peak at a value that is larger than one, around a defined threshold of receptor concentration. Reaching this threshold, a little change of n_R causes a rapid change in the fraction of bound particles[5].

The analytical model of Martinez-Veracoechea and Frenkel demonstrated that the peak value of α increases with the decrease of binding strength, indicating that weak bonds are more selective than strong ones. Indeed, if the individual binding is strong, NPs will bind to all the receptors available and the surface would be saturated regardless of their receptor concentration thus not allowing super selectivity. Due to their instability, weak bounds unlikely bind surfaces with low concentration. On the other hand, increasing n_R, the number of simultaneous bonds increases, making the overall binding stronger[5].

It is also possible to analyze how the fraction of surface that is occupied by the ligand changes increasing the number of receptors. **Figure 1.7** represents the output of this

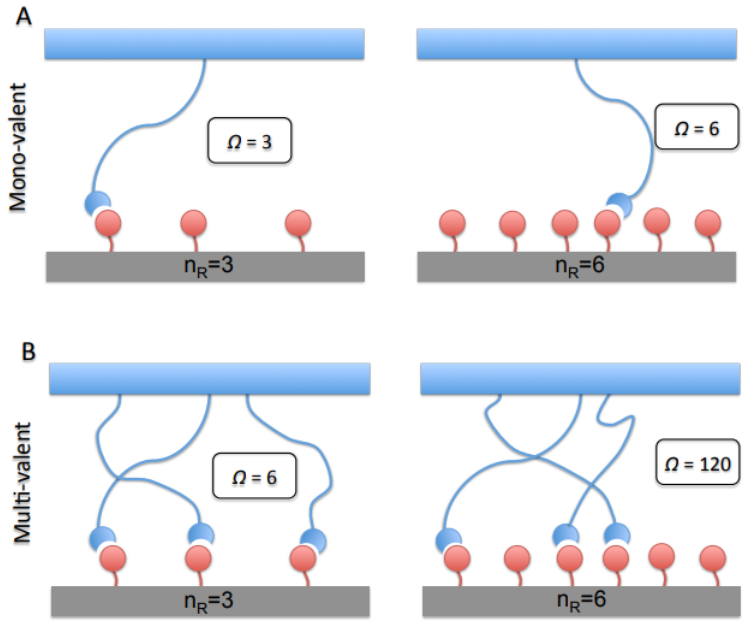

Figure 1.6: Entropic influence in super selectivity: considering a flexible binding, where each of the k ligand can bind to every one of the nR receptors. The picture represents the binding in (A) monovalent and (B) a multivalent cases, in both non-overexpressing (left) and overexpressin (right) situation. In the case of univalent system, the degeneracy factor Ω grow linearily with the number of receptors, indeed, in the case of multivalency the increase is non-linear and much more relevant [4].

model, taking into consideration two monovalent and one multivalent system.

Thus, the monovalent systems cannot give selectivity, as the fraction of ligand bound varies slowly with the increasing of n_R. On the other hand, this selectivity is achieved through the multivalent system, where NPs only bind significantly to high concentrated surfaces, while leaving the surfaces with a low expression of the receptor almost untouched.

In this scenario, it is possible to identify an upper limit to the number of ligands to tether on the NPs. An increasing number of interacting ligands could, in fact, hinder the binding. This happens because every ligand introduces a certain repulsion due to its steric hindrance. More ligands, thus, bring more repulsion, which could not be counterbalanced by the increase in the attractive contribution to the binding free-energy [36].

To sum up, the interaction between the ligand and receptor can be adjusted to achieve a low level of affinity that is necessary for highly selective targeting. To create a strong

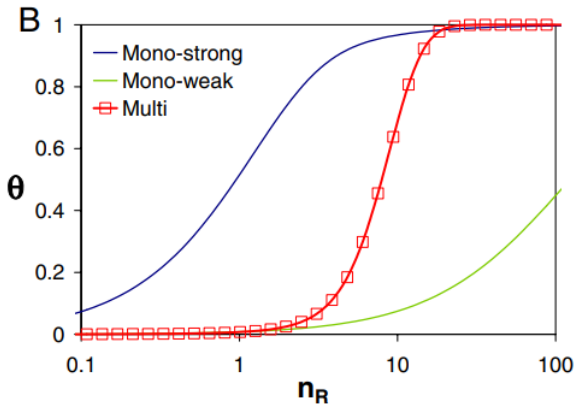

Figure 1.7: Results of the analytical model: comparison between a multivalent system, a strong monovalent, and a weak monovalent one. The multivalent on shows an almost "on-off" behavior[5].

platform for targeting specific cells that overexpress a unique receptor, it is necessary to combine the appropriate particle size, number of ligands, length of the polymer brush, ligand affinity, and receptor volume in a multiplexed system.

1.4 PEG-PLA polymersomes

Polymersomes (POs) are amphiphilic block co-polymer, that can self-assemble into vesicles when hydrated. The self-assembly is mainly caused by non-covalent interaction (van der Waals forces) of the hydrophobic block. The hydrophobic blocks of the chains tend to interact with each other, avoiding water contact, while the hydrophilic blocks face the water inside and outside the vesicle delimiting the two interfaces of a bilayer membrane[37]. The structure of POs is represented in **Figure 1.8**.
To produce POs utilizing amphiphilic blocks, various parameters need to be optimized, including concentration, molecular weight, polymer geometry, and block ratios. The size of the resulting structures is influenced by the amphiphilicity of the co-polymer, as well as the specific self-assembly preparation methods employed. Additionally, external factors such as extrusion, sonication, or freeze/thaw cycles can further influence the POs' structure[38]. Overall, the POs' performance is predominantly dependent on the block co-polymer chemistry[39]. Active moieties, including peptides, proteins, and antibodies, can be incorporated onto the surface of POs to introduce additional characteristics. This enables the precise design of POs for targeted drug delivery and superselective targeting,

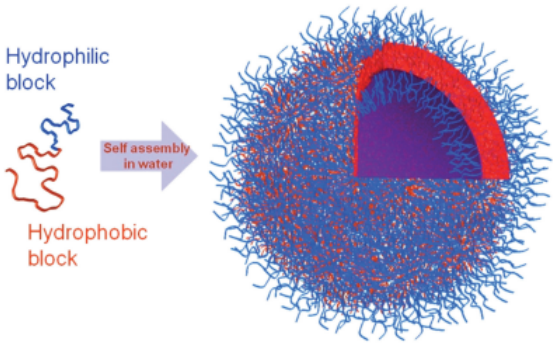

Figure 1.8: 3D structure of polymersomes[6].

enhancing their overall effectiveness[6].

In the last decade, POs have emerged as a promising drug delivery system (DDS) as they offer several key features that make them highly advantageous compared to other DDSs:

- Are composed of biocompatible and biodegradable materials, which reduces the likelihood of adverse reactions or toxicity.
- Provide superior size and shape control, enabling fine-tuning of nanoparticles via the modulation of their chemical properties and manufacturing protocols.
- Can facilitate controlled drug release, thereby reducing the chances of adverse side effects.
- Offer exceptional stability by safeguarding drugs from premature degradation and release, thereby enhancing their efficacy and safety.
- Can be easily functionalized with various targeting moieties, such as antibodies or peptides, allowing for targeted drug delivery.
- Can be produced at large scales utilizing simple and cost-effective methods, making them a highly attractive option for drug delivery applications.

One example of the amphiphilic co-polymer used for POs formulation is PEG-PLA. PEG (polyethylene glycol) is the hydrophilic block, it is biocompatible, and resistant to immunological recognition and to phagocytosis. PEG is metabolized by oxidation of the alcohol group to form a carboxylic acid, diacids and metabolites of hydroxyl acid in presence of enzyme-catalyzed alcohol dehydrogenase. The hydrophobic block in

question is polylactic acid (PLA), which degrades through hydrolysis into a non-toxic hydroxyl-carboxylic acid that is further metabolized into water and carbon dioxide, resulting in complete biodegradation[40]. On the other hand, PLA is characterized by poor hydrophylicity and so by poor hydrophulic drug loading, that could be completely compensated by synthesising PEG-PLA block copolymer. In addition to this, the presence of a PEG brush on POs surface increase their biological stability, decreasing the immune reactivity, and thus leading to a prolonged systemic circulation. Ultimately, in vivo assays proved PEG-PLA copolymer to be highly tolerable and not accumulative at low concentrations[41].

2. Aim of the work

The aim of this thesis project was to investigate the use of ligand multivalency to achieve superselectivity in target HER2 receptors on cancer cells. We hypothesized that by using multivalent ligands, we can achieve a higher degree of specificity in binding HER2 receptors, which are overexpressed on the surface of many cancer cells. In fact, in multivalent interactions a particular PO uses multiple ligands to bind simultaneously to several receptors on cell surface. In this way is possible to create interactions that depends on the amount of receptors in the cell surface, and on the number of ligands used to functionalise the PO, allowing a discrimination between healthy cells and cancer cells to avoid the side effects of conventional therapies. This work was focused on the use of PEG-PLA POs conjugated with KCCYSL, a synthetic peptide derived from phage display libraries, that is able to target HER2 receptor.

The primary objective of this study is to conjugate KCCYSL peptide to the PEG-PLA co-polymer chain to prepare polymersomes that exhibit this ligand specific for HER2 receptor. Subsequently, we assessed the expression levels of the HER2 receptor on patient derived GBM cells, by protein quantification assays. This enabled us to estimate the binding interactions between the POs and the cells with known receptor concentration. Subsequently, we investigated the binding efficacy of KCCYSL decorated POs in distinct cell types that exhibit varying levels of HER2 receptor expression, such as GBM and HER2-positive breast cancer cells. The aim of this analysis was to assess the selectivity of the POs as a drug delivery system and/or as a treatment, while considering factors such as the number of ligands attached and the concentration of the targeted receptor. Eventually, we checked the viability on the cells that have been exposed to KCCYSL to determine if the binding of these POs can potentially interfere with HER2 signaling, consequently inducing apoptosis and cell death. In this way we determined the ability of KCCYSL decorated POs in inhibiting the growth and survival of cancer cells that express the HER2 receptor.

3. Materials and methods

3.1 Conjugation of PEG-PLA and KCCYSL

$Pra-KCCYSL$ (U9660HG280, Genscript) was conjugated to $N_3-PEG_{20}-PLA_{106}$ by exploiting the copper(I)-catalyzed 1,3-dipolar cycloaddition of alkynes and azides to synthesize 1,2,3-triazoles. Specifically, 80.85 mg (1 molar equivalent) of $N_3-PEG_{20}-PLA_{106}$ dissolved in 5.39 ml of DMF (227056-1L, Merck) were mixed to 10 mg (1,3 molar equivalents) of $Pra-KCCYSL$ dissolved in 0.33 ml of water. Then, 9.4 mg (5 molar equivalents) of Sodium Ascorbate [$C_6H_7NaO_6$, (A7631-25G, Sigma Aldrich)] dissolved in 0.05 ml of water were added to form Solution 1. To catalyze the reaction, 30 mg of Copper Sulfate [$CuSO_45H_2O$, (1027805000, Sigma Aldrich)] were dissolved in 3 ml of water (Solution 2). Both the solutions were then purged with nitrogen for 1 hour. Then, 0.24 ml (1 equivalent) of Sol. 2 were added to Sol. 1 without allowing air to flow inside the flasks. Then the mix was left under constant stirring for 72 hours (Big Squid, IKA). The suspension was then loaded into a 3.5 kDa dialysis membrane (11495869, MWCO Spectrum Labs), previously sterilised in 70% (v/v) ethanol (1310861611, Panreac) for 24 hours and washed with sterile milli-Q water. To remove the unreacted product and the organic solvent, the sample was dialysed against DMF for 2 hours and then against milli-Q water for 72 hours. After the dialysis the sample was freeze-dried overnight.

3.1.1 Conjugation efficiency

To calculate the conjugation efficiency the KCCYSL conjugated polymer and the pure KCCYSL peptide (Genscript) were hydrolyzed, then dissolved in 1.0 M Hydrochloric Acid [HCl, (10000180, Fisher Chemical)] to a final concentration of $1.39{\cdot}10^{-8}$ mol/ml and finally the obtained aminoacids were derivatised to allow the detection through HPLC. To determine the quantity of the peptide bound to the polymer chain, the peaks of the amminoacids in the conjugated polymer were compared to the peaks of the pure peptide. The process is explained in details in the sequent subsections.

3.1.1.1 Hydrolysis

The hydrolysis solvent was prepared by mixing trifluoracetic acid [TFA, (11404863, Alfa Aesar)] and HCl with a ratio TFA:HCl equal to 1:2. The standard and the testing solutions were prepared by dissolving respectively the pure KCCYSL pepetide and KCCYSL-PEG-PLA in the hydrolysis solvent (HS), to a final number of mols of $4.20 \cdot 10^{-8}$.
From the standard and the testing solutions, 600 μl were loaded to the vacuum hydrolysis tube (TS-29571, Thermo Scientific). The tube was then evacuated with vacuum three times, heated at 166 °C in the oil bath (1069005000, Supelco) for 50 minutes and cooled down at room temperature.
Then, the solvent was evaporated by vacuum pump, fitted with a trap and liquid nitrogen to freeze the acid. After a complete evaporation of the solvent, 900 μl of 0.1 M HCl were used to dissolve the hydrolyzed sample. Then the solution was heated at 120 °C till it started boiling. Finally, the samples were collected from the tube to 1.5 ml HPLC vials (SVC2-W02-100, Metria, provided by Aparatos Normalizados S.A.). By this step, all the reconstituted sample solutions were at a molar concentration of $1.39 \cdot 10^{-8}$ mol/ml.

3.1.1.2 Derivatization

To derivatise the reconstituted samples, AccQ Fluor Reagent Kit purchased by Waters (WAT052880) was used. Both the pure peptide and the polymer conjugated peptide were treated as suggested by the manufacturer. To form the final derivatised sample, 1050 μl of buffer, 150 μl of 2B reagent solvent (acetonitrile), 150 μl of AccQ reagent and 150 μl of reconstituted sample solution were transferred to a 1.5 ml HPLC vial. At this point the concentration of the derivatised sample was of $1.39 \cdot 10^{-9}$ mol/ml. The vials were vortexed for 10 seconds and then put on a heated block for 10 minutes. The blank was prepared by blending 1200 μl of buffer with 300 μl of 2B reagent solvent.

3.1.1.3 High Performance Liquid Chromatography (HPLC)

The derivatives were separated by reverse phase High Performance Liquid Chromatography and the fluorescence of the labeled amminoacids was detected. For this analysis a Dionex Ultimate 3000 was used. The samples and the blanks were loaded on the HPLC with water as Solvent A and 70 % (v/v in water) HPLC grade acetonitrile (ACTN-0GH-P04, Labkem) as Solvent B. Settings used for the run are showed in **Table 3.1**.

Flow rate	1 ml/min
Temperature	37 °C
Time	48
Excitation wavelength	250 nm
Emission wavelength	395 nm
Gain	1
Filter	0.5

Table 3.1: HPLC settings

3.1.1.4 Calculation

The amount of conjugated KCCYSL was calculated by a calibration curve analyzing the area of the peak of leucine in the unconjugated peptide. The conjugation efficiency was then calculated with the following equation:

$$Conjugation\,efficiency\,(\%) = \frac{A_p}{A_p + (c \cdot V_i \cdot 10^7 - A_p \cdot M_{w1}) : M_{w2}} \times 100$$

Where A_p is the amount of KCCYSL in pmol, c is the mass concentration of the derivatised conjugate sample in $\mu g/\mu l$, V_i is the volume injected in the HPLC in μl, M_{w1} is the molar mass of the conjugated polymer and M_{w2} is the molar mass of the unconjugated polymer in g/mol.

3.2 Conjugation of PEG-PLA and Cy5

$Pra - Cy5$ (C70B0, Lumiprobe GMBH) was conjugated to $N_3 - PEG_{20} - PLA_{106}$ following the same procedure described in **Section 3.1**. Specifically, 235.65 mg of $N_3 - PEG_{20} - PLA_{106}$ dissolved in 11.8 ml ml of DMF were mixed to 20 mg of $Pra - Cy5$ dissolved in 1 ml of water. Then, 27.4 mg of Sodium Ascorbate dissolved in 0.68 ml of water were added to form Solution 1. Solution 2 was formed as described previously (see **Section 3.1**). After purging the solution, 0.69 ml of Sol.2 were added to Sol.1 without allowing air to flow inside the flaks.The sample was then dialyzed and freeze-dried according to the standard protocol.

3.3 Polymersomes preparation - Solvent displacement method

A standard solvent displacement protocol for PEG-PLA was used to prepare seven different formulations of polymerosomes funtionalized with multiple ligands. Briefly, $KCCYSL-PEG_{20}-PLA_{106}$, $Cy5-PEG_{20}-PLA_{106}$ and $MeO-PEG_{45}-PLA_{106}$ were dissolved in DMF to form solution 1, solution 2 and solution 3 respectively at a concentration of 5 mg/ml, 20 mg/ml and 60 mg/ml. The seven final formulations were obtained by mixing the three solutions according to what summarized in **Table 3.2**, to obtain a final polymer concentration of 20 mg/ml. Under sterile conditions, 0.8 ml of

Molar % of KCCYSL	Sol.1 (ml)	Sol.2 (ml)	Sol.3 (ml)	DMF (ml)
0 %	0	95	301.7	603
0.2 %	19.6	95	300	586
0.5 %	48.9	95	297.5	559
0.7 %	68.4	95	295.8	541
1 %	97.8	95	293.3	514
2 %	195.5	95	284.9	425
5 %	488.9	95	259.7	157

Table 3.2: Polymersomes formulations

the organic solution of the copolymer were injected into 1.867 ml of sterile milli-Q water under magnetic stirring at 500 rpm. The injection was performed through a syringe pump (NE-1000, New Era Pump Systems Inc.) with flow rate set at 100 $\mu l/min$. A 30% (v/v) of the copolymer was obtained at the end of the injection. The suspension was then dyalized into a 3.5 kDa dialysis membrane, previously sterilized in 70% (v/v) ethanol for 24 hours and washed with sterile milli-Q water. To remove the organic solvent, the sample was dialysed against sterile milli-Q water for the first hour and then against sterile PBS 1X (18912014, Life Technologies) overnight. After the dialysis the formulations were further purified. First, every sample was centrifuged at 1000 rcf for 10 minutes (Centrifuge 5810 R, Eppendorf), then the supernatant was loaded into a size-exclusion chromatography (SEC) column and collected into a 96-well plate (see **Section 3.4.2**). The collected sample was then characterized as described in **Section 3.5**.

3.4 Size Exclusion Chromatography (SEC)

3.4.1 Column preparation

First of all, the SEC columns (C3919, Supelco) were washed with ethanol 70% for 24 hours, and Sepharose (GE17-0120-01, Sigma Aldrich) was left in a 50 ml falcon with ethanol 70% for 24 hours. After 24 hours, Sepharose was centrifuged at 3000 rcf for 5 minutes to remove ethanol and then washed with sterile milli-Q three times. The washing process was then repeated three more times by using sterile PBS 1X (10010056, Gibco). Finally, Sepharose was dissolved in PBS and poured into the SEC columns under sterile conditions. After that the Sepharose was completely packed, the columns were washed three times with sterile PBS.

3.4.2 Sample purification

A maximum of 2 ml of sample were loaded into the SEC column for each run and sterile PBS was used to elute it. The sample was then collected into 96-well plates, approximately to 200 μl per well. Between different formulations, the SEC column was washed with sterile PBS three times.

The first particles being eluted from the SEC column are the biggest ones, while the smaller ones are trapped in the Sepharose and eluted later. Indeed, the sample recovered is generally divided into three fractions: a first one containing bigger nanoparticles and aggregates, a second one containing smaller nanoparticles and a third one with even smaller and more diluted nanoparticles. The second fraction was then collected to obtain a more homogeneous sample containing polymerosomes with medium size.

3.5 Polymersomes characterization

POs were then characterized by dynamic light scattering (DLS), high performance chromatography (HPLC) and transmission electron microscopy (TEM).

3.5.1 Dynamic Light Scattering

The size and polydispersity of PEG-PLA POs were analysed by DLS using a Zetasizer Ultra (Malvern Panalytical). The instrument works with a He-Ne laser at 633 nm, the temperature was set at 25 °C and the scattered light was measured at an angle of 173°. To prepare the samples, 10 μl of the formulations were diluted with 70 μl of sterile PBS and transferred into polystyrene disposable microcuvettes (BR759200-100EA, Sigma).

Results were analysed using ZS Explorer Software by Malvern Panalytical and GraphPad Prism 8 Software.

3.5.1.1 Number of ligands

The number of ligands per polymersome was calculated according to what described in a previous work[42]. The calculation was based on the size distribution derived from DLS data and on the molar percentage of KCCYSL-PEG-PLA of each formulation.

3.5.2 High Performance Liquid Chromatography

To calculate the concentration of polymersomes, the samples were analysed by HPLC using a UV-Vis absorbance detector. The amount of polymer in the polymersomes formulations was calculated creating a standard curve based on the copolymer solution (see **Section 3.3**.). For this analysis a Agilent 1260 Infinity II was used.

3.5.2.1 Experimental Section

Specifically, to prepare the standard curve samples, 50 μl of the pristine solution (copolymers concentrated at 20 mg/ml in DMF) were diluted in 950 μl of a solution 1:1 of HPLC grade acetonitrile (ACN) and water, to a final concentration of 1 mg/ml. A solution made of 50 μl of DMF and 950 μl of ACN:water 1:1 was used as a blank for the standard curve. To prepare the polymersomes samples, 50 μl of each formulation were diluted in 250 μl of a solution 1:1 of acetonitrile (ACN) and water. In this case, 1000 μl of ACN:water 1:1 were used as a blank. The samples were then transferred into HPLC vials and loaded into the instrument. The sequence used to analyse the samples is described in **Table 3.3**. Before and after the run of the samples, the column was washed with 0,1% (v/v in water) sodium dodecyl sulfate [SDS, (436143, Sigma Aldrich)] and pure HPLC grade acetonitrile.

3.5.2.2 Analysis

The analysis was based on the area of the peak of PEG-PLA polymer absorbance. First of all, the spectra of the blanks were subtracted to the spectra of the samples. A standard curve was created by associating the injected mass, calculated from the injected volume and the concentration (1 mg/ml), with the area of the peak. With the calibration curve it was possible to associate the area of the peaks, derived from the analysis of the

Sample	**Quantity** (μl)
0.1% SDS	100
Blank standard curve	100
Blank standard curve	100
Sample standard curve	20
Sample standard curve	40
Sample standard curve	60
Sample standard curve	80
Sample standard curve	100
Blank formulations	100
Blank formulations	100
Sample 0% KCCYSL	100
Sample 0.2% KCCYSL	100
Sample 0.5% KCCYSL	100
Sample 0.7% KCCYSL	100
Sample 1% KCCYSL	100
Sample 2% KCCYSL	100
Sample 5% KCCYSL	100
0.1% SDS	100
ACN (washing)	100

Table 3.3: Sequence for samples analysis in HPLC

formulations, with the injected mass. Known the injected volume and the injected mass, the concentration of each formulation was calculated.

3.5.3 Transmission Electron Microscopy

All the formulation were previously diluted 1:3 in sterile PBS and transferred in 600 μl eppendorf tubes. The samples were then sonicated for 5 minutes in ice in a XUB5 Digital Ultrasonic Bath (Grant Instruments) to avoid aggregates. For the imaging, carbon-coated copper grids were used (C300Cu100 EMresolution TEM-CF300CU50 Merck). Before sample loading, the grids were glow-discharged for 30 seconds to make the surface hydrophilic. Then, 6 μl of the diluted samples were loaded on the grids for 1 minute. Subsequently, the grids was blotted with filter paper and negatively stained by soaking into 0.5% (w/v) phosphotungstic acid (PTA) pH 7 for 3 seconds or into Uranyless EM Stain (22409, Uranyless) for 30 seconds.

The PTA staining solution was previously prepared by dissolving 25 mg of phosphotungstic acid (79690-25G, Sigma) with 5 mL of boiling distilled water under constant stirring. The pH was adjusted to 7.0 with 5M NaOH (SOHY-P0T-1K0, Labkem) and left under stirring for 5 minutes. Then, the solution was filtered through 0.2 μl filter (SLGP033RS, Merck Millipore).

After being stained, the grids were blotted with filter paper and dried with vacuum. Grids were then imaged using an EM JEOL J1010 at 80 kV at the Electron Cryomicroscopy Unit of the University of Barcelona (CCiTUB, Barcelona, Spain).

3.6 Cell culture

GBM2 are patient derived primary cells kindly donated by from Antonio Daga, and were cultured and maintained in Neurobasal Medium (12348017, TermoFisher), DMEM F12 (12634010, ThermoFisher) and DMEM high glucose (11965092, Gibco) mixed with a ratio of 2:1:1. The basal medium was supplemented with 2% of B27 supplement (17504044, ThermoFisher), 1% of of L-Glutamine (25030024, Gibco), 1% of insulin, 0.1% of EGF, 0.1% of FGF and 0.1% of of Heparin (H3393-10KU, Sigma). Previously, insulin solution was prepared by dissolving insulin from bovine pancreas (I5500-50MG, ThermoFisher) in filtered milli-Q water to a concentration of 2 mg/ml, adjusting the pH to 2/2.3 with HCl and then adjusting the volume with milli-Q water to a final concentration of 1.5 mg/ml. EGF solution was prepared by dissolving 100 μl of Animal-Free Recombinant Human EGF (AF-100-15, Peprotech) in 500 μl of milli-Q water and 4500 μl of sterile

PBS 1X (10010056, Gibco). FGF solution was prepared by dissolving 10 μl of Recombinant Human FGF (100-18B, Peprotech) in 50 μl of Tris solution 5mM pH 7.6 and 450 μl of sterile PBS 1X 0.1% BSA (A2153-50G, Sigma Aldrich). For the experiments, cells were washed with sterile DPBS (14190144, Thermofisher) and detached with TrypLE Express Enzyme (12604013, Thermo Fisher). To allow the cells to adhere, flasks and wells were previously coated with matrigel for 1 hour at 37 °C. Specifically, Corning Matrigel Growth Factor Reduced (GFR) Basement Membrane Matrix (354230, ThermoFisher) was dissolved in DMEM F-12 to a final concentration of 0.05%.

U87 cells, purchased from ATCC were cultured and maintained in Eagle's Minimum Essential Medium (ATCC, 30-2003) supplemented with 10% FBS (10270-106, Life Technologies,S.A.) and Blaticidine (12172530, ThermoFisher) to a final concentration of 8 $\mu g/ml$.

Sk-Br-3, purchased by ATCC were cultured and maintained in McCoy's 5a modified medium (EP-CM-L0238, bionova cientifica) supplied with supplemented with 10% FBS, 1% penicillin-streptomycin, and 5 % of 100 mM sodium pyruvate (11.360.039, Gibco)

For the experiments, U87, and Sk-Br-3 cells were washed with sterile PBS 1X and detached with Trypsin-EDTA 0.05% (25300-062, Gibco).

3.7 Extraction of Protein Content

To prepare samples for protein quantification, GBM2 cells, U87 cells, and Sk-Br-3 cells were cultured in T25 flasks. When cells were confluent the medium was aspired, then the cells were washed with sterile PBS 1X for two times and then scraped with a sterile cell scraper (PLC90021, SPL Life Sciences) in 5 ml of PBS 1X. Then cells were collected and centrifuged. Subsequently, the obtained cell pellet was washed two times with PBS 1X and frozen at −80 °C. To extract proteins from cell pellet, a Cell Extraction Buffer 1X was prepared by mixing Cell Extraction Buffer PTR 5X (ab193970, Abcam) and Cell Extraction Enhancer Solution 50X (ab193971, Abcam) in deionized water, with dilution of respectively 1:5 and 1:50. The buffer was then supplemented with 1% of protease inhibitor cocktail (P8849, Sigma). Cell pellet was dissolved in 200 μl of Cell Extraction Buffer 1X and cell lysates were transferred into 2 ml eppendorf tubes and incubated on ice for 20 minutes. After 20 minutes, samples were centrifuged at 18000 rcf for 20 minutes at 4 °C. The supernatant obtained was used for the assays and then stored at −80 °C.

3.8 BCA Protein Quantification Assay

To quantify the total protein content in every cell line, a BCA Assay kit purchased from ThermoScientific (23225), was used. The samples were prepared by diluting the protein extract in Cell Extraction Buffer 1X, both prepared as described in **Section 3.7**, to reach a final dilution of 1:5. To prepare the standard, Bovine Serum Albumine [BSA, (A2153, Sigma Aldrich)] was dissolved in Cell Extraction Buffer 1X, to a final concentration of 2 mg/ml. To obtain a standard curve, serial dilutions 1:2 (from 2 mg/ml to 0,001 mg/ml) were performed. Then, protein content was quantified according to the manufacturer's instructions. Briefly 25 μl of the standards and the unknown samples were transferred in the proper wells of transparent 96-well plates. Then, 200 μl of working reagent were added to each well, mixed for 30 seconds and incubated for 30 minutes at 37 °C. The working reagent was previously prepared by mixing 50 parts of Reagent B to 1 part of Reagent A. After the incubation, the plated was cooled down at room temperature, and then absorbance at 562 was read nm on a microplate reader (Spark® TECAN).

3.9 ELISA Assay

To calculate the basal content of HER2 receptor in each cell line, an ELISA kit, purchased by Abcam (ab283881) was used. All the reagents and the standards were prepared according to the manufacturer's instructions. The samples were prepared as described in **Section 3.7** and further diluted with Cell Extraction Buffer 1X. The final protein concentrations used for the assay are summarized in **Table 3.4**. A schematic description of the assay is illustrated in **Figure 3.1**. By using a standard curve associating HER2 expression to the absorbance, it was possible to calculate the amount of HER2 receptor in each sample. The results were then normalized to the total protein content calculate as described in **Section 3.8**.

Cell line	**Concentration** ($\mu g/ml$)
GBM2	55
U87	74
Sk-Br-3	0.44

Table 3.4: Protein concentrations for ELISA Assay

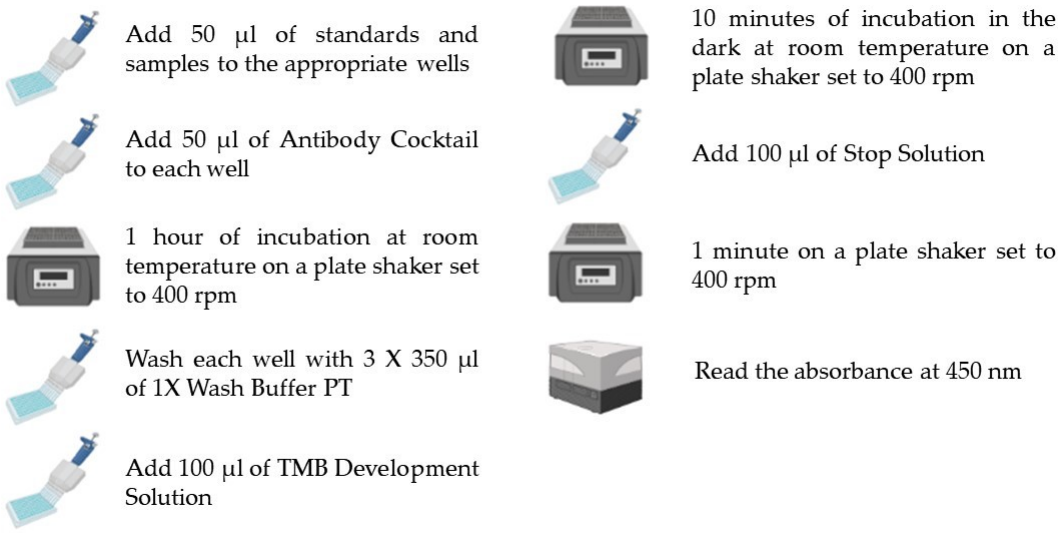

Figure 3.1: Schematic illustration of ELISA assay protocol. Created with Biorender

3.10 Immunofluorescence Assay

The presence of HER2 receptor in GBM2 cells and Sk-Br-3 cells has been evaluated also by immunofluorescence. Cells were seeded on glass coverslips (631-0153, VWR) and cultured until 80% of confluence, and then washed three times with PBS 1X and fixed with PFA 4% (252931.1214, Panreac) for 10 minutes at room temperature. To block unspecific interactions, a blocking step was performed by incubating the cells with PBS 1X + 2% BSA for 1 hour at room temperature. Then, the cells were first incubated with the primary antibody diluted [AbI, (2165S, Cell signaling technology)] 1:200 in PBS 1X + 2% BSA overnight at 4°C, followed by three washes with PBS 1X and subsequent incubation with the secondary antibody [AbII, (Alexa Fluor® 568)] diluted 1:500 in PBS 1X + 2% BSA at room temperature for 2 hours. Cells were then washed three times with PBS 1X, and stained with HOECHST (11534886, Invitrogen) diluted 1:2000 in PBS 1X at room temperature for 10 minutes. The samples were then mounted on a coverslip with Fluoromount (0100-01, Southern Biotech) and let at room temperature to dry for at least 2 hours. Fluorescence was detected on a Leica TCS SP8 confocal laser scanning microscope. All images acquired were taken with a 63x objective. AbII fluorescence was excited with a Diode laser at 578 nm and emission was detected at 603

nm (IDEM) while HOECHST fluorescence was excited with the same laser at 350 nm and emission was detected at 461 nm.

3.11 MTT Assay

The metabolic activity of cells was assessed using the MTT [3-(4,5-dimethylthiazol-2-yl)-2,5-diphenyltetrazolium bromide] assay purchased by Invitrogen (M6494).

3.11.1 Polymersomes toxicity

Cells were seeded at a density of 10.000 cells per well in transparent 96-well plates 24 hours. The protocol consists in treating cells with different concentrations (from 952226 to 6250000000 NPs/μl) of KCCYSL functionalised polymersomes (KCCYSL-POs) for 2 hours and 24 hours. Then, the POs solution was removed and cells were incubated with the MTT solution (0,5 mg/ml in sterile PBS) for 2 hours at 37 °C. After the removal of the MTT solution, 50 μl of DMSO (472301-1L, Sigma Aldrich) was added to each well to dissolve the formazan crystals. Absorbance was measured using a microplate reader at 570 nm with a reference wavelenght of 630 nm. The percentage of cell viability was obtained by comparing the absorbance of treated cells with non treated cells, incubated with normal cell medium. Positive control was obtained by treating cells with 20% DMSO v/v in sterile PBS.

3.11.2 KCCYSL toxicity

The same protocol described in **Section 3.11.1** was applied to asses the metabolic activity of the cells upon treatment with KCCYSL peptide. In this case, cells were treated for 24 hours with different concentration of KCCYSL dissolved in sterile PBS 1X, starting from 140 μM to 4.4 μM with serial dilution 1:2. After 24 hours the MTT assay was performed and analyzed as described before.

3.12 Binding Assay

To analyze the binding ability of the different formulations of KCCYSL-POs, GBM2 cells and Sk-Br-3 cells were seeded at a density of 20.000 cells per well in respectively black (M9685-100EA, Greiner) and transparent 96-wells plates. After 24 hours cells were treated with KCCYSL-POs at a concentration of $1{\cdot}10^7$ NPs/μl, and incubated at 37 °C. When reached a specific time point, the supernatant was collected and transferred to a

black 96-well plate, while the cells were stained with HOECHST diluted 1:2000 in sterile PBS for 20 minutes at room temperature. The fluorescence of the collected supernatant was read at the microplate reader, the excitation wavelength was set to 633 nm and the emission wavelength to 677 nm, with a band width of 20 nm. Supernatant was collected and read at a time point 0 (only nanoparticles at a concentration of $1{\cdot}10^7$ NPs/μl) and then after 30 minutes, 1 hour and 2 hours. Number of nanoparticles and fluorescence were associated with a standard curve, allowing then the calculation of the POs bound to the cells. Once obtained the number of NPs for each time point, these values were subtracted to the value of the time point 0 to obtain the number of polymersomes bound to the cell.

To calculate the number of cells in each well, a standard curve associating the number of cells to the fluorescence of HOECHST was built, by seeding cells at a different concentration (from 80.000 to 2.500 cells/well). After 4 hours, cells were stained with HOECHST diluted 1:2000 in sterile PBS for 20 minutes at room temperature. The fluorescence of HOECHST was read at the plate reader, with excitation set to 350 nm and emission to 461 nm. The final data is then expressed as number of POs per cell.

4. Results and discussion

4.1 KCCYSL-PEG-PLA polymersomes

To prepare the POs decorated with our ligand of interest, KCCYSL peptide was conjugated to the PEG-PLA block co-polymer by the click chemistry.

4.1.1 Ligand conjugation

The click chemistry consists of the copper-catalyzed azide-alkyne cycloaddition (CuAAC) ligation process. This reaction was used to conjugate the alkyne-KCCYSL to the azide-PEG-PLA, as illustrated in **Figure 4.1**. The azide group is linked to the hydrophilic block of the co-polymer, allowing the peptide to be exposed once that the POs are formed.

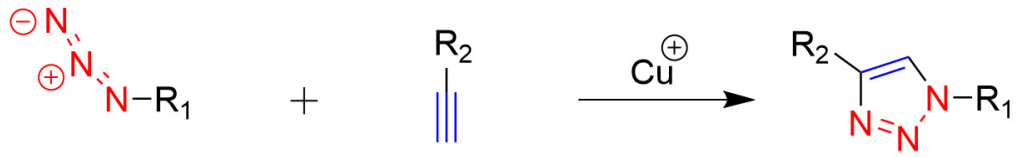

Figure 4.1: Schematic representation of the click-chemistry process: the polymer with a terminal azide group is conjugated with the peptide with an alkyne group through a Cu(I) catalyst. R_1 is the block co-polymer, R_2 is the peptide.

The reaction proceeds by first activating the azide group with the copper catalyst, facilitating the formation of a reactive intermediate, which reacts with the alkyne group to form a 1,2,3-triazole ring. The reaction was left under stirring for 72 hours, until the complete depletion of the reagents.

Then, the solution was dialysed against DMF and water to remove the organic solvent and unreacted products. After the purification process the solution was freeze-dried and stocked.

To calculate the conjugation efficiency, and so the amount of peptide in the reaction that was successfully conjugated to the polymer, the pure KCCYSL peptide (sample 1) and the peptide conjugated to the block co-polymer (sample 2) were hydrolyzed, derivatized and then analyzed through the HPLC as described in the material and method section. Based on a previous work[43], we determined the area of the peak of leucine (see **Figure 4.2**), one of the amminoacids composing the peptide, in order to compare the amount of the ligand in sample 1 and 2. The area of leucine in the KCCYSL conjugated co-polymer is significantly lower compared to the pure peptide (**Table 4.1**), meaning that part of the ligand in the reaction did not conjugate.

The parameters involved in the calculation of the conjugation efficiency (CE) are summarized in the **Table 4.2**, where A_p is the amount of KCCYSL conjugated to PEG-PLA, c is the mass concentration of the derivatized conjugate sample, V_i is the volume injected in the HPLC, M_{w1} is the molar mass of the conjugated polymer and M_w2 is the molar mass of the unconjugated polymer.

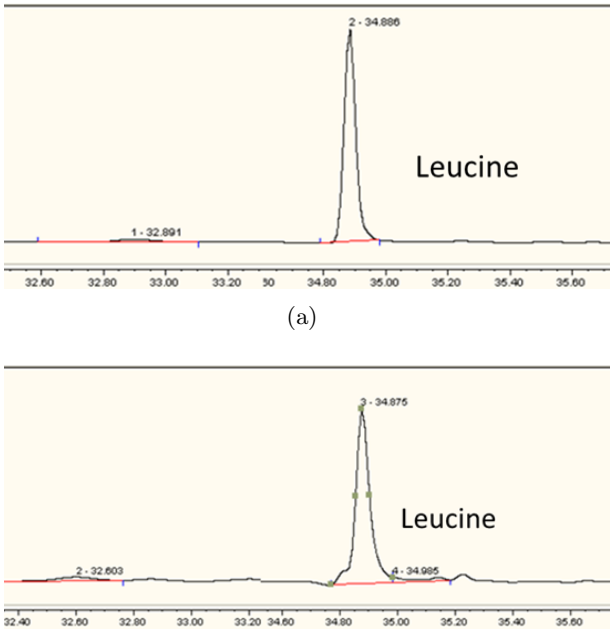

Figure 4.2: HPLC output: the picture (a) shows the peak of leucine in the pure KCCYSL peptide, while (b) shows the same peak derived from the peptide that was previously linked to the PEG-PLA chain. The area of leucine peak in (b) is lower, meaning that not all the peptide in the reaction was conjugated.

The final conjugation efficiency (CE) was calculated as the mean of the five percentages

Pure KCCYSL		**KCCYSL-PEG-PLA**	
Volume injected (μl)	**Area (LU·s)**	**Volume injected (μl)**	**Area (LU·s)**
100	44804208.87	100	8830335.877
80	32735531.69	80	7072009.56
60	22500007.07	60	5073927.976
40	13114957.46	40	3540213.294
20	6329419.159	20	1805832.894

Table 4.1: Output of the HPLC: the table shows the area calculated through integration in the case of the pure peptide and the KCCYSL conjugated polymer.

$A_p(pmol)$	$V_i(\mu l)$	$M_{w1}(g/mol)$	$M_{w2}(g/mol)$	$c(\mu g/\mu l)$
133.39	100			
116.43	80			
97.16	60	9329.86	8519.36	0.043
82.37	40			
65.6	20			

Table 4.2: Parameters used to calculate the conjugation efficiency: KCCYSL content, mass concentration of derivatized sample, volume injected and molar masses of conjugated and unconjugated polymer.

obtained by using the different values of A_p and V_i with the following equation:

$$CE_j\ (\%) = \frac{A_{pj}}{A_{pj} + (0.043\mu g/\mu l \cdot V_{ij} \cdot 10^7 - A_{pj} \cdot 9329.86 g/mol) : 8519.36 g/mol} \times 100$$

$$\bar{CE} = 39.9\%$$

The conjugation efficiency of the click chemistry is known to be correlated with the nature of the solvent, as demonstrated by Shiraghi et al. in 2021[44]. In this study water showed a yield of 95% in 1 hour of reaction, compared to a yield of 5% after 4 hours for DMF in the same condition. The authors also demonstrated that mixing the organic solvent with water can allow a better conjugation efficiency[44]. In the present work, the reaction solution for KCCYSL-PEG-PLA conjugation was composed of 5.98 ml of DMF and 0.62 ml of water, that, in 72 hours of reaction allowed a high conjugation efficiency (39%). Reducing the amount of the organic solvent was not possible due to the non solubility of $N_3 - PEG_{45} - PLA106$ in water.

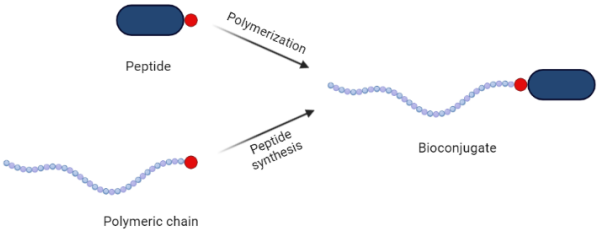

(a) Divergent conjugation

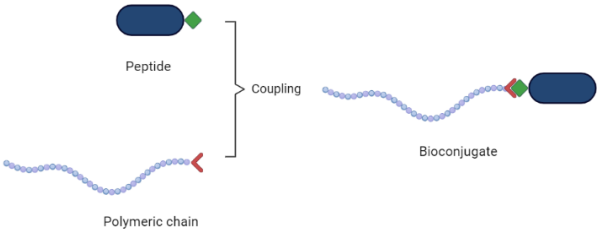

(b) Convergent conjugation

Figure 4.3: Bioconjugation processes. In the divergent (a) process one of the two components is built from the other, while in the covergent one (b) the peptide and the polymer chain are synthesized separately and then attached to each others[7]. Created with BioRender.

In the last decades research was focusing on exploiting directly nature's building blocks such as peptides and proteins in order to generate biomimetic materials[45]. Peptides and proteins are indeed characterized by a great variety of functionalities but, on the other hand, also by low solubility, high sensitivity to temperature and pH, and by a short circulation time *in vivo*. These limitations can be overcome by the conjugation with selected synthetic polymers[7] such as polyethers and polyesters, characterizing then a new promising class of biomaterials[45].

The bioconjugation process should preserve the intrinsic properties of biomolecules, thereby avoiding any potential alteration or modification of its physicochemical and biological characteristics. The possible processes have been divided into two main classes, the divergent and the convergent routes[46], briefly explained in **Figure 4.3**.

In the divergent process the synthetic polymer is grown directly from the peptide segment, or the peptide is sequentially assembled on the synthetic polymer[47]. Therefore, divergent processes have several limitations, such as a difficult purification and isolation of the two components, needed to analyze and characterize the bioconjugate[7]. These complications can be overcome by using convergent methods, in which the polymer chain

and the peptide are synthesized separately and then coupled exploiting one or more reactive sites. Convergent approaches allow a separate synthesis and characterization of the components, making easier the final analysis.

One of the most successful coupling reactions in recent years, was the "click" cycloaddition azide/alkyne reaction[47]. By employing this reaction, it became feasible to distinguish between the two constituents (the block co-polymer and the peptide), facilitating a comparative analysis between the pure peptide utilized for the conjugation process and the peptide bound to the block co-polymer. This enabled the quantification of the conjugation efficiency. The yield of the process was considered for the accurate incorporation of KCCYSL-PEG-PLA chains into the co-polymer mix during polymersome formulation. Indeed, a derivatization factor was computed based on the conjugation efficiency to determine the actual percentage of KCCYSL-PEG-PLA needed to achieve the target molar ratios of KCCYSL in the POs.

4.1.2 Polymersomes formulation

Polymersomes were prepared by solvent displacement method. Briefly, the organic solutions composed of $MaO-PEG_{45}-PLA106$, $Cy5-PEG_{20}-PLA_{106}$, and $KCCYSL-PEG_{20}-PLA_{106}$ at different molar percentages were injected into sterile milli-Q water to reach a co-polymer concentration of 30% (v/v) in the final volume. At the end of the injection, the suspensions of nanoparticles exhibited a milky appearance, as shown in **Figure 4.4**, indicating the existence of nanoparticles that were forming a colloidal suspension.

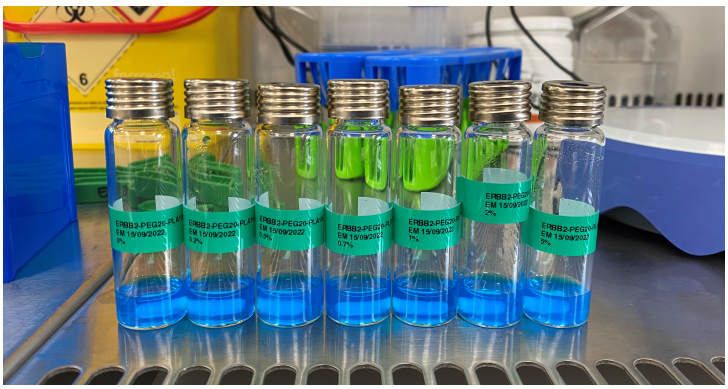

Figure 4.4: Polymersomes formulations. The picture shows the seven different formulations obtained by solvent displacement technique, the blue color is due to the presence of the Cy5 while the milky appearance demonstrates the formation of the NPs.

The suspensions were then dialyzed overnight and purified according to the standard protocol. After centrifugation and SEC, used to remove any undesired structures, the formulations were characterized by DLS, TEM and HPLC.

Although various methods have been studied for POs purification[48], centrifugation was selected to purify particles according to their shape, sice non spherical POs are characterized by a larger polymer/water ratio and so by a higher density. As a second step SEC was employed to separate POs based on their size, allowing a separation into monodisperse fractions. This way a more homogeneous sample is obtained, allowing a better characterization of size and shape.

4.1.3 Polymersomes characterization

Part of the samples were diluted 1:8 and analyzed by DLS, to evaluate the size, the homogeneity, and to calculate the number of ligands for each formulation. To confirm the DLS data and to check the morphology of the POs, TEM analysis was performed as described before (see **Section 3.5.3**). The POs concentration in each sample was analyzed by HPLC.

The quality of the sample can be demonstrated from the correlograms of the formulations (**Figure 4.5**). The cart in the picture shows a rapidly decaying signal, meaning that the samples do not present aggregates and can be considered monodisperse. Moreover, **Figure 4.6** demonstrates that, regardless of KCCYSL incorporation, the different formulations are composed of POs with comparable size (100-120 nm) in agreement with previous reports[53,52]. These data are also confirmed by the TEM images (**Figure 4.7**), which illustrate sphere-like vesicles with a mean size comparable to the results obtained by DLS. POs concentrations were comparable to each other, ranging from 3.30 mg/ml and 5.50 mg/ml. All the characterization measurements are summarized in **Table 4.3**. The formulation method, together with the purification processes, allowed the formation of homogeneous and monodisperse POs with spherical shape.

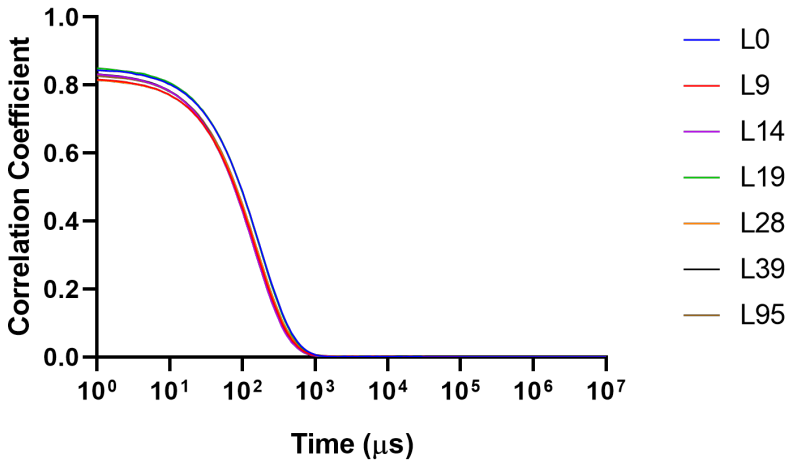

Figure 4.5: Correlogram: the correlation functions indicate the quality of the sample in analysis. Overall, the sample does not show aggregates and can be considered monodisperse.

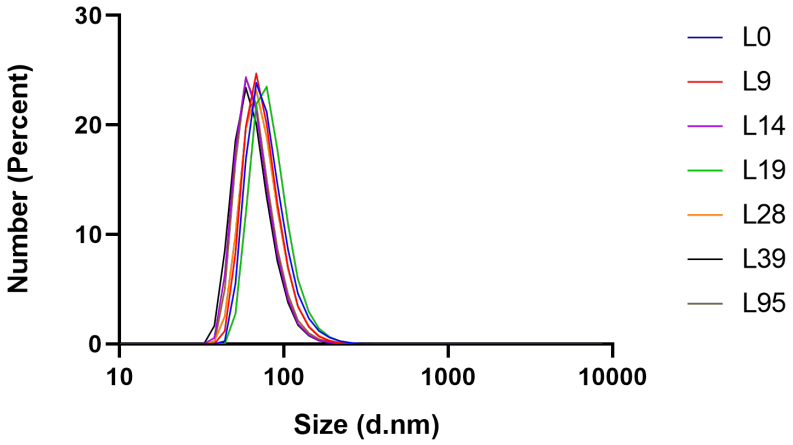

Figure 4.6: Size distribution: the chart shows the size distribution of the POs to the number of particles (%). The mean size of the formulations ranges between 100 and 120 nm.

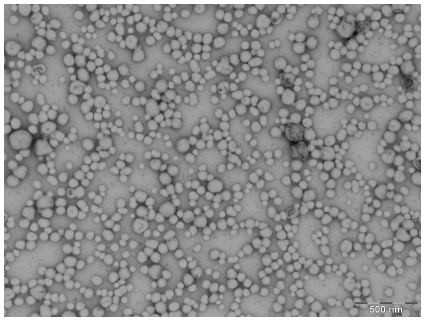

(a) 0% KCCYSL

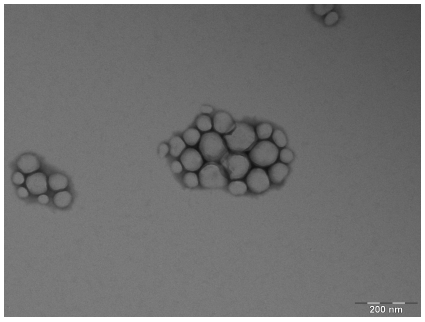

(b) 0.2% KCCYSL

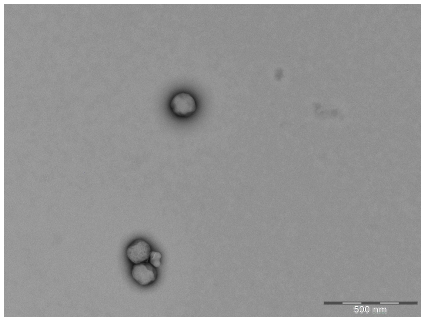

(c) 0.5% KCCYSL

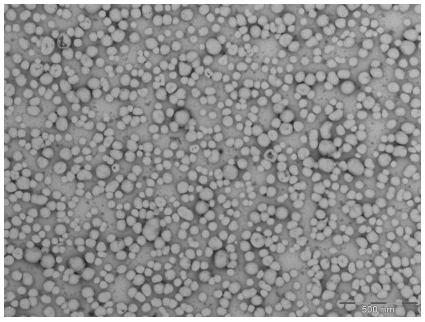

(d) 0.7% KCCYSL

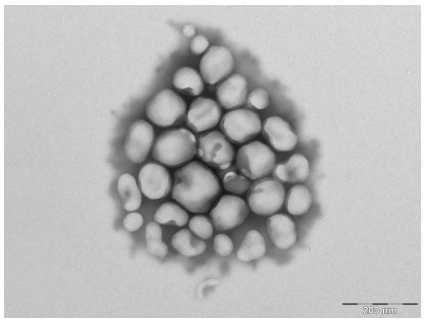

(e) 1% KCCYSL

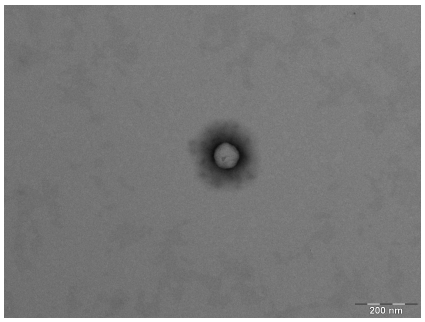

(f) 2% KCCYSL

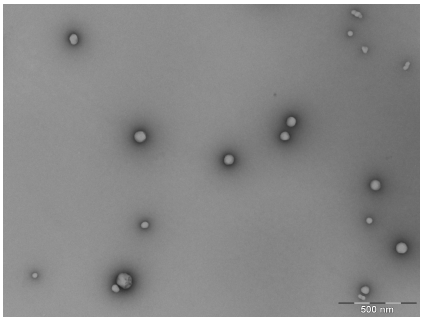

(g) 5% KCCYSL

Figure 4.7: TEM images: the grids were prepared following the described protocol (see **Section 3.5.3**). The grids (a) and (d) were stained using PTA 0.5% while the grids (b), (c), (e), (f) and (g) were stained using Uranyless EM stain.

Formulation	**Number of ligands**	**Mean size** (nm)	**Concentration** (mg/ml)
0% KCCYSL	0	119.6	5.50
0.2% KCCYSL	9	103.1	3.71
0.5% KCCYSL	19	118.1	5.48
0.7% KCCYSL	14	99.9	3.72
1% KCCYSL	28	112.6	4.39
2% KCCYSL	39	100.6	3.56
5% KCCYSL	95	107.1	3.29

Table 4.3: POs characterization after DLS and HPLC analysis.

4.2 HER2 quantification

To evaluate HER2 basal expression, three different cell lines were cultured and analyzed. GBM2 and U87 cells were employed as *in vitro* sample of glioblastoma, while Sk-Br-3 cells were used as positive control, as they are a breast cancer cell line known in literature to express high levels of HER2[49].

4.2.1 BCA assay

In order to calculate the amount of HER2 receptor per mg of proteins, the total protein content was calculated by a standard BCA assay. The analysis was then performed by creating a standard curve from a sample of known concentration. The results of the analysis are summarized in **Table 4.4**.

Cell line	**Protein content (mg/ml)**
GBM2	4.7
U87	2.3
Sk-Br-3	3.7

Table 4.4: Total protein content quantified by BCA assay

4.2.2 ELISA assay and immunofluorescence

An ELISA assay was performed as a first quantitative evaluation of HER2 basal expression of GBM2, U87 and Sk-Br-3 cells. The assay was carried on as described in materials and methods (**Section 3.9**) analyzing the absorbance of each sample by a

standard curve generated from pure HER2 protein at known concentration. The data obtained were then normalized to the total protein content calculated by BCA, to express the amount of HER2 receptor over the total protein content.

To have a qualitative evaluation of HER2 content, GBM2 cells and Sk-Br-3 cells where stained with a primary antibody specific to HER2 receptor and a secondary antibody specific to the primary antibody. The fluorescence of the secondary antibody was then detected by laser confocal microscope. As showed in **Figure 4.8**, GBM2 and U87 cells contain respectively 2.8 and 5.2 pg of HER2 every μg of proteins, compared to the 1000 $pg/\mu l$ of our positive control (Sk-Br-3).

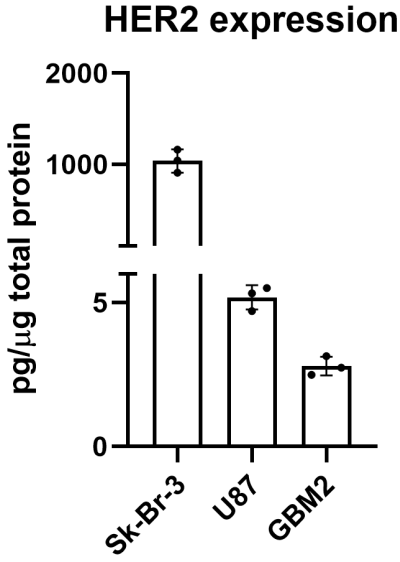

Figure 4.8: HER2 quantification by ELISA assay: the chart demonstrates an overexpression of HER2 receptor in Sk-Br-3 cells compared to GBM2 and U87 cells.

The quantitative analysis of the ELISA assay was used to verify HER2 expression in cancer cells using Sk-Br-3 as positive control. Indeed the last are well known to overexpress HER2 receptor[49].

This difference of expression between Sk-Br-3 and GBM2 cells is also shown by the microscopy imaging (**Figure 4.9**).

In order to investigate how superselectivity works depending on the amount of receptor expressed on the cell surfaces, all subsequent experiments were carried on always comparing both HER2-overexpressing cells (Sk-Br-3) and non-overexpressing cells

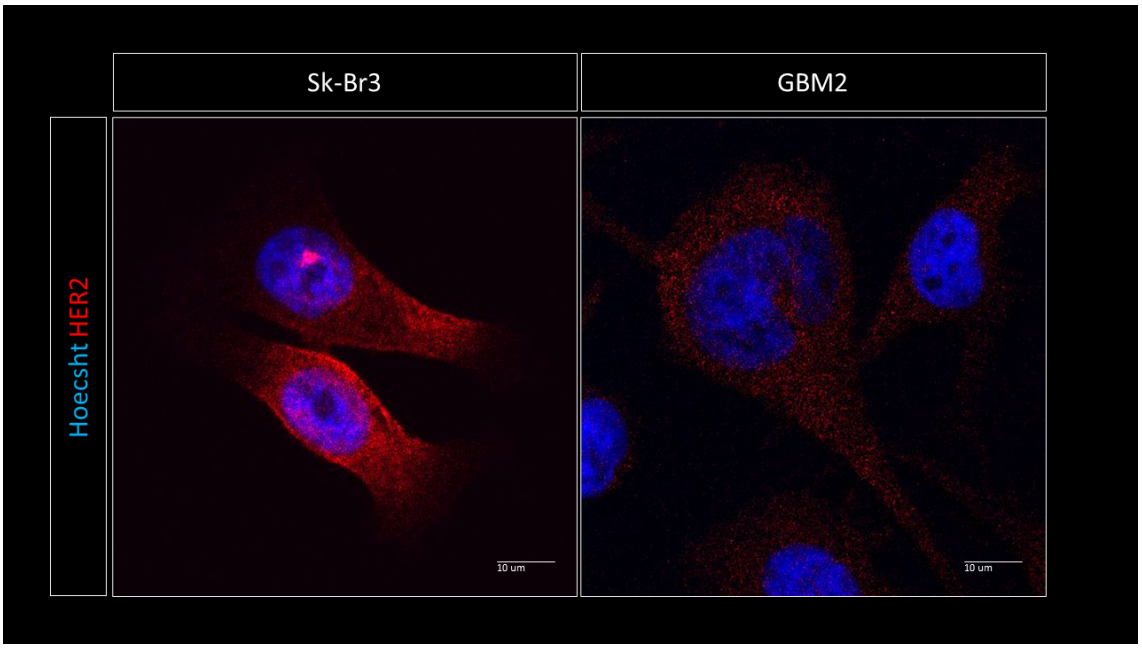

Figure 4.9: HER2 evaluation with microscopic techniques: the images confirmed the data of the ELISA assay.

(GBM2). The aim of this work was in fact to evaluate the interaction between POs and cells, specifically by examining the effect of the number of ligands tethered on the POs' surface and the concentration of receptors on cell surfaces.

4.3 Cell viability

The objective of this assay is to determine whether targeting the HER2 receptor with KCCYSL peptide can interfere with receptor dimerization and so with its ability to promote cell proliferation. To evaluate cellular toxicity upon POs treatment, the metabolic activity of cells was assessed by MTT assay, a common method used to measure cell viability or proliferation. The assay relies on the ability of living cells to reduce the tetrazolium salt, MTT, into formazan crystals, which are insoluble in water. The amount of formazan produced is proportional to the number of viable cells in the culture. To evaluate the amount of formazan produced, its absorbance was read by plate reader at 570 nm.

Therefore, absorbance of formazan produced by cells treated for 2h and 24h with different concentrations of POs was compared to the one of untreated cells. The percentage

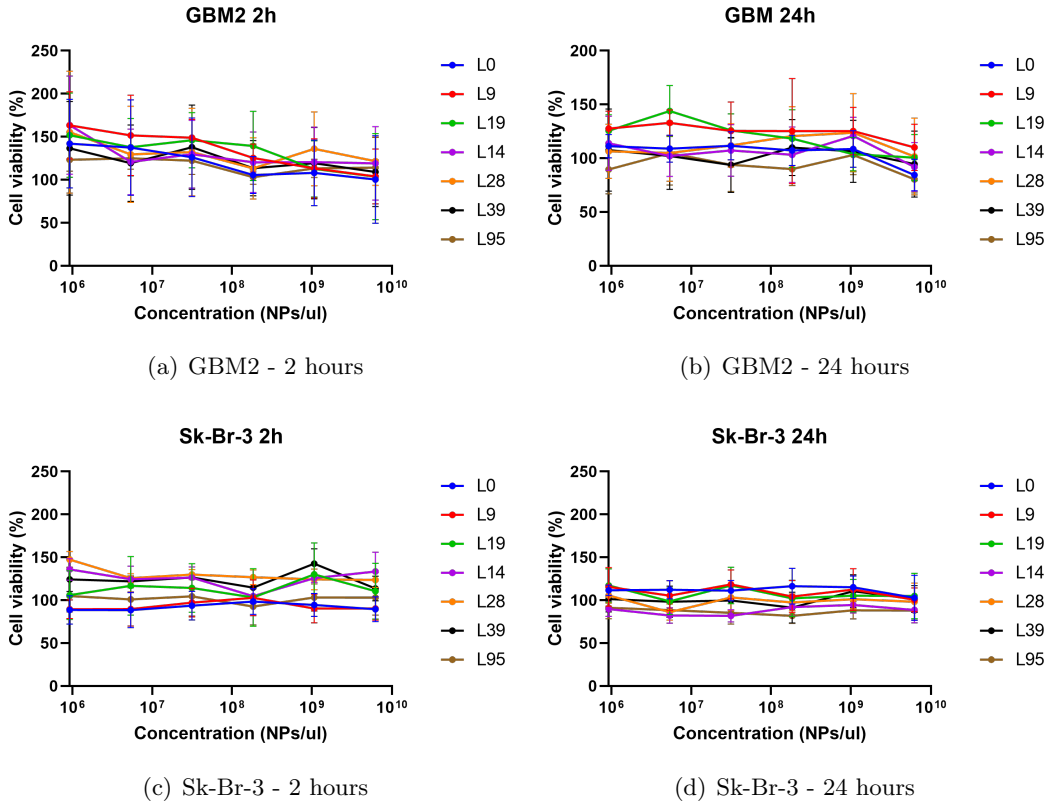

(a) GBM2 - 2 hours

(b) GBM2 - 24 hours

(c) Sk-Br-3 - 2 hours

(d) Sk-Br-3 - 24 hours

Figure 4.10: POs citotoxicity: the minimum value obtained by the MTT assay analysis is 70% of cell viability, thus not indicating cellular toxicity.

of viable cell was calculated by the following equation:

$$Cell\ viability\ (\%) = \frac{OD\ 570nm\ treated\ cells}{OD\ 570nm\ untreated\ cells} \times 100$$

A reduction of cell viability less or equal to 30% was not considered cellular toxicity.

As illustrated in **Figure 4.10**, no toxicity effect has been observed upon the treatment with KCCYSL decorated POs both in GBM2 and Sk-Br-3 cells. This unexpected result can be explained by the low binding capability of the POs. If the peptide is unable to effectively bind to the cells, it cannot interfere with the receptor's dimerization ability, thereby limiting its biological activity. Indeed, although binding occurred correctly, the lack of cell toxicity may occur due to the peptide's binding site, which may differ from the site of dimerization, leading to a correct binding without altering the receptor's signaling activity. In order to evaluate if this lack of biological effect was

due to the peptide or to how the peptide is linked with the POs, the metabolic activity of GBM2 and Sk-Br-3 was also evaluated by treating the cells only with the peptide. KCCYSL was dissolved in cell medium at different concentration to treat the cells. The MTT assay was performed 24 hours after, following the standard protocol.

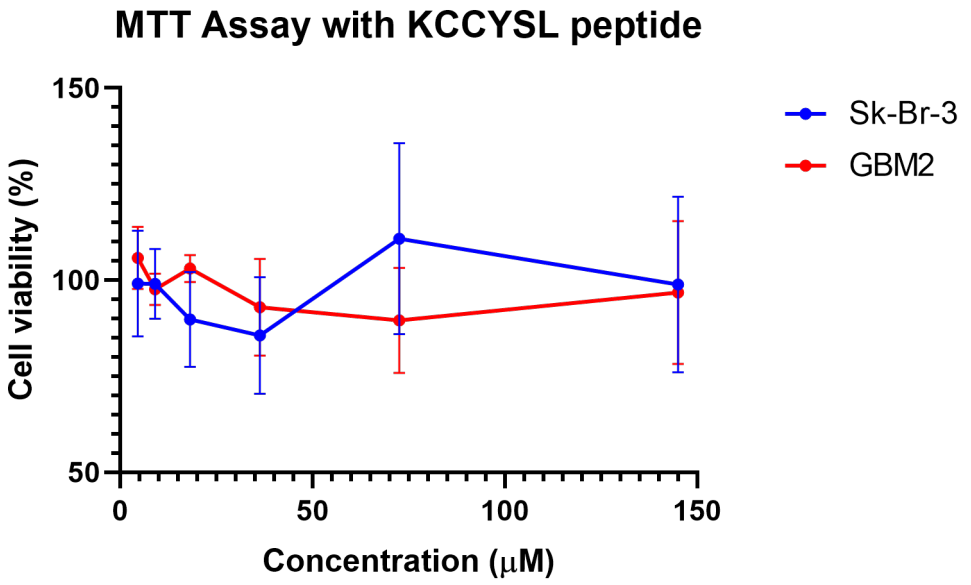

Figure 4.11: Peptide citotoxicity: the minimum values of cell viability for GBM2 and Sk-Br-3 were respectively of 85% and 89%, thus indicating the absence of toxicity.

Also in this case, the treatment with the peptide did not cause significant effect on cell viability on both cell lines, as demonstrated by the chart in **Figure 4.11**. The absence of citotoxicity tends to confirm the hypothesis of a different binding domain compared to the one of receptor dimerization.

Based on this analysis, the hypothesis of inducing cellular toxicity using KCCYSL can be rejected. However, the peptide can still be employed to target cancer cells. Previous studies have demonstrated the effectiveness of KCCYSL-decorated liposomes in targeting HER2 receptors as MRI contrast agents[51], as well as the use of KCCYSL labeled with radiotracers such as ^{64}Cu as radiopharmaceuticals for imaging HER2-expressing tumors[52].

The ability of POs to target cancer cells was then studied with a binding assay, performed to evaluate the super selectivity both on Sk-Br-3 and on GBM2 cells using different POs formulations.

4.4 Binding assay

To evaluate the binding capability of KCCYSL decorated POs, a binding assay was performed by incubating the cells with the formulations at different time points (30 minutes, 1 hour, 2 hours), and then measuring the fluorescence of the supernatant. The number of POs bound to the cells was calculated by subtracting the fluorescence of POs in the supernatant to the value obtained at 0 time point. Then, the value was normalized by the number of cells per well, to eventually express it in number of POs per cell.

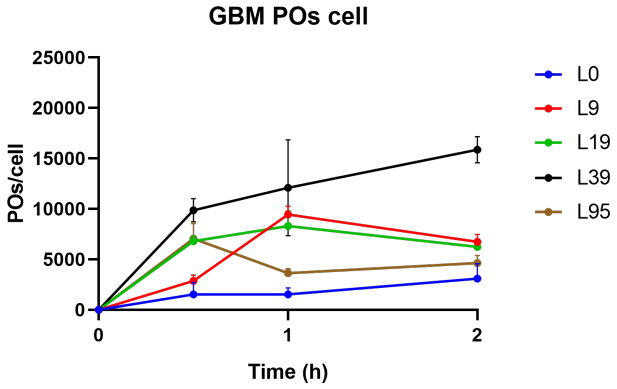

(a)

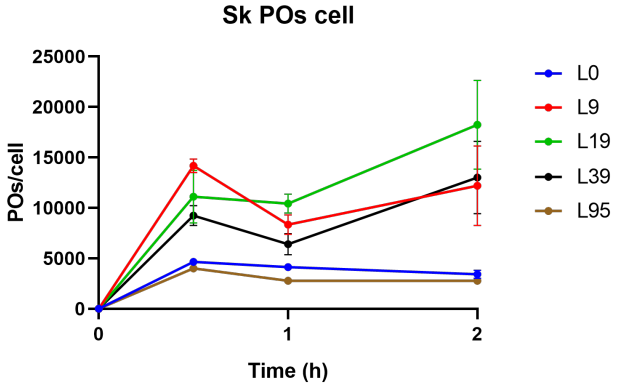

(b)

Figure 4.12: Binding assay: the charts represent the number of POs bound to each cell depending on the time of exposition. In the case of GBM2 cells (a) L39 is the formulation which shows better interaction, while in Sk-Br-3 (b) the same is observed with L19.

Based on the results depicted in **Figure 4.12**, it is evident that the absence of ligands

in L0 leads to a lack of interaction with the HER2 receptor, as expected in both the cell types. The weak interaction noticed is, most probably, due to non specific interaction of PEG-PLA nanoparticles, as observed also in previous studies[53]. The enhanced interaction observed between the other formulations and the cells can be attributed to the presence of KCCYSL ligands that facilitate the binding with the HER2 receptor. However, it is noteworthy that L95 formulation displays poor interaction with both Sk-Br-3 and GBM2 cells, thus indicating that the steric hindrance between the ligands inhibits the binding.

In order to better understand the interaction within the different formulations and the cells, **Figure 4.13** represents how the POs bind with the cell surface depending on the number of ligands tethered on their surface.

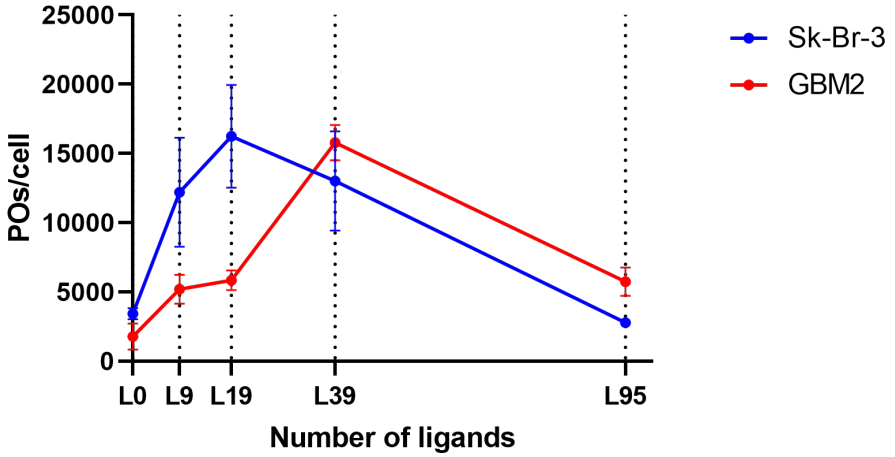

Figure 4.13: Binding selectivity: the chart represents how ligand multivalency influences the binding capability of the NPs.

The amount of POs per cell increased as we increased the number of ligands, until reaching a certain maximum, where a decreasing started. In fact, L0 and L95 have almost the same binding avidity, showing that having too many ligands tethered on the POs surface does not allow a stronger binding. This behavior confirmed that few weak interactions are not enough to achieve a proper binding, while by increasing the number of ligands an higher number of POs per cell can be uptaken. On the other hand, as previously studied[29], keeping increasing the number of ligands does not assure a better binding, due to the steric hindrance of the peptides which causes repulsion and interfere with the ligand-receptor interaction.

The graphical representations illustrate that there is a consistent level of binding observed in both cell types. Specifically, there does not appear to be a correlation between the receptor overexpression and the number of POs bound per cell. However, a notable difference in the maximum binding effect is evident among the specific formulations. In Sk-Br-3 cells, the maximum binding effect is achieved with L19, whereas in GBM2 cells, with L39. These results suggest that a greater number of weak interactions are required to achieve stable binding in cells that do not overexpress receptors, such as GBM2, as compared to HER2 overexpressing cells, such as Sk-Br-3.

Additionally, it is noteworthy that in Sk-Br-3 cells, formulations L9 and L39 exhibit considerable binding efficacy. This suggests that, in the context of overexpression, the variance in binding efficiency between the different formulations is comparatively less significant when compared to normal expression. This enables the achievement of better binding in case of overexpression by using different formulations that do not bind to other cells, thereby avoiding side effects.

In the specific case of GBM2 cells, a sharper response of POs per cell to the number of ligands is observed. Indeed, a successful binding can be achieved using only one of the five formulations tested (L39), but the amount of POs per cell is comparable to the one of Sk-Br-3 cells.

Cells with various expression of HER2 receptor interact differently with different formulations of KCCYSL decorated POs. In particular, by manipulating the number of ligands based on the receptor concentration a super selective binding could be achieved. Therefore determining the expression of HER2 receptor, an optimal number of peptides tethered to POs' surfaces could be identified.

5. Conclusion and future perspectives

The objective of this study was to create a super selective system using KCCYSL ligand tethered on the surface of POs, with the ability to specifically target HER2 receptor in GBM cells. POs were selected as vectors with improved mechanical properties and colloidal stability compared to other nanoparticles, such as liposomes[54]. In this study, a PEG-PLA block co-polymer was employed as an amphiphilic base, owing to its great biocompatibility and stealth properties[55].

First, the expression of HER2 receptor on different lines of GBM cells was confirmed[29] through immunological techniques, exploiting Sk-Br-3 as positive control. Subsequently, the investigation was extended to evaluate the interaction between the system under study and cells with different receptor concentration.

The interaction between the POs and the cells was investigated through binding assay and MTT assay. It was demonstrated that super selectivity can be achieved on both cell types, by exploiting formulations with different number of ligands. In details, L39 was more selective to GBM2 cells, while L19 interacted more with Sk-Br-3 cells. However, through the binding to HER2 receptor, it was not possible to interfere with its ability to enhance cell proliferation and survival. The MTT assay, indeed, demonstrated no cellular toxicity upon the treatment with all the formulations, and the same results were achieved using a treatment with the peptide alone, indicating that KCCYSL binding site differs from receptor dimerization site. POs were then able to selectively bind GBM cells, thus not inducing cell death.

In conclusion, KCCYSL decorated POs could be potentially exploited as a drug delivery system. Indeed, the efficiency of PEG-PLA nanoparticles is well recognized thanks to its great properties, such as (1) an increased bioavailability *in vivo*, (2) increased drug loading and encapsulation efficiency, (3) enhanced systemic circulation, and (4) biocompatibility[41]. Moreover, in POs, the dissociation and consequent release of the encapsulated drug is triggered by the internalization within the target cell.

In such context, KCCYSL peptide can be integrated as it can be simply conjugated

to the PEG-PLA diblock through convergent techniques and it allows to target HER2 receptor in a selective way, as demonstrated in this work.

In this study, it was observed that the interaction under investigation could potentially be enhanced by optimizing the properties of the POs. Although a binding effect was detected, the current number of POs per cell was found to be relatively low. Further optimization of the POs properties could therefore lead to a more efficient interaction and potentially improve the overall effectiveness of the system.

The overall avidity of the system could be increased through the reduction of steric potential that arises from the presence of the polymer brush on the external surface of the PO[42]. This reduction in steric hindrance would allow for greater accessibility of the ligand, ultimately resulting in a more efficient interaction between the ligand and the targeted receptor.

Furthermore, the interaction between KCCYSL-POs and healthy cells needs to be investigated, in order to evaluate possible side effects. Then, this system could be employed as a vector to target specific drugs to cancer cells leaving normal cells untouched.

6. Aknowledgments

First of all, I would like to express my gratitude to the Institute of Bioengineering of Catalonia for the opportunity to access their laboratories.

I would like to thank Giuseppe Battaglia; since the first meeting, I knew that something in my life was changing forever. Thank you for this amazing opportunity and for those that will come next. I would also like to thank all the members of the Molecular Bionics group for helping me with this project and for making me feel at home, always. You will be in my heart forever.

I would like to thank my supervisor, Matilde, for being my guide, teacher, and friend. I will always treasure the moments we spent together inside and outside the lab, and I will never be able to thank you enough. My gratitude also goes to Catia Lopes for teaching me with passion; it was an honor to learn from you.

I would like to thank my relator, Gianluca Ciardelli, for trusting me and helping me with patience even though I am not the most organized student, and co-relator Clara Mattu.

All my gratitude goes to my family. You shared every moment of this long journey with me, with love and patience, and I feel blessed every day to have your support.

Special thanks to the other half of my heart, Domiziana, for always being with me and supporting me unconditionally. Thank you, Pagghi, for being with me since forever. When I told you about this thesis, your eyes made me understand that I was doing something big, and I promise you that I will always put all my efforts into this job.

My gratitude also goes to Daniele, Sabrina, Arianna, Martina, Martina, and all my friends from Brandizzo, for always being there for me, even when I was not. Wherever I go, you will be home forever.

I want to express my gratitude to the best team I have ever had: Irene, Ylenia, Valentina, Alessio, and to the man who made everything possible, Savio. Thank you for making me who I am today; I wouldn't be the same without you.

Finally, I would like to thank Leonardo for coming back into my life and becoming so much in such a short time, and my Italian twin, Francesca. Knowing you is one of the best gifts that life gave me during these crazy two years. Thank you for your constant support and your precious friendship.

7. Bibliography

1. Robert Roskoski Jr. The erbb/her receptor protein-tyrosine kinases and cancer. *Biochemical and biophysical research communications*, 319(1):1–11, 2004.

2. Cristina Marchini, Lucia Pietrella, Cristina Kalogris, Chiara Garulli, Federico Gabrielli, Elena Quaglino, Manuela Iezzi, Serenella M Pupa, Elda Tagliabue, and Augusto Amici. Her2-driven carcinogenesis: New mouse models for novel immunotherapies. In *Oncogene and Cancer-From Bench to Clinic*. IntechOpen, 2013.

3. Wanyi Tai, Rubi Mahato, and Kun Cheng. The role of her2 in cancer therapy and targeted drug delivery. *Journal of controlled release*, 146(3):264–275, 2010.

4. Tine Curk, Jure Dobnikar, and Daan Frenkel. Design principles for super selectivity using multivalent interactions. *Multivalency: Concepts, Research & Applications*, pages 75–101, 2018.

5. Francisco J Martinez-Veracoechea and Daan Frenkel. Designing super selectivity in multivalent nano-particle binding. *Proceedings of the National Academy of Sciences*, 108(27):10963–10968, 2011.

6. Caterina LoPresti, Hannah Lomas, Marzia Massignani, Thomas Smart, and Giuseppe Battaglia. Polymersomes: nature inspired nanometer sized compartments. *Journal of Materials Chemistry*, 19(22):3576–3590, 2009.

7. Sabrina Dehn, Robert Chapman, Katrina A Jolliffe, and Sébastien Perrier. Synthetic strategies for the design of peptide/polymer conjugates. *Polymer Reviews*, 51(2):214–234, 2011.

8. Quinn T Ostrom, Mackenzie Price, Corey Neff, Gino Cioffi, Kristin A Waite, Carol Kruchko, and Jill S Barnholtz-Sloan. Cbtrus statistical report: Primary brain and other central nervous system tumors diagnosed in the united states in 2015–2019. *Neuro-oncology*, 24(Supplement_5):v1–v95, 2022.

9. Frank B Furnari, Tim Fenton, Robert M Bachoo, Akitake Mukasa, Jayne M Stommel, Alexander Stegh, William C Hahn, Keith L Ligon, David N Louis, Cameron Brennan, et al. Malignant astrocytic glioma: genetics, biology, and paths to treatment. *Genes & development*, 21(21):2683–2710, 2007.

10. Anoop P Patel, Itay Tirosh, John J Trombetta, Alex K Shalek, Shawn M Gillespie, Hiroaki Wakimoto, Daniel P Cahill, Brian V Nahed, William T Curry, Robert L Martuza, et al. Single-cell rna-seq highlights intratumoral heterogeneity in primary glioblastoma. *Science*, 344(6190):1396–1401, 2014.

11. Diana Matias, Joana Balça-Silva, Grazielle C da Graça, Caroline M Wanjiru, Lucy W Macharia, Carla Pires Nascimento, Natalia R Roque, Juliana M Coelho-Aguiar, Cláudia M Pereira, Marcos F Dos Santos, et al. Microglia/astrocytes–glioblastoma crosstalk: crucial molecular mechanisms and microenvironmental factors. *Frontiers in cellular neuroscience*, 12:235, 2018.

12. Hans-Georg Wirsching and Michael Weller. Glioblastoma. *Malignant Brain Tumors: State-of-the-Art Treatment*, pages 265–288, 2017.

13. Mary Elizabeth Davis. Glioblastoma: overview of disease and treatment. *Clinical journal of oncology nursing*, 20(5):S2, 2016.

14. Kaja Urbańska, Justyna Sokołowska, Maciej Szmidt, and Paweł Sysa. Glioblastoma multiforme–an overview. *Contemporary Oncology/Współczesna Onkologia*, 18(5):307–312, 2014.

15. Patrick Y Wen and Santosh Kesari. Malignant gliomas in adults. *New England Journal of Medicine*, 359(5):492–507, 2008.

16. Patrick Y Wen and Alba A Brandes. Treatment of recurrent high-grade gliomas. *Current opinion in neurology*, 22(6):657–664, 2009.

17. Erwin G Van Meir, Costas G Hadjipanayis, Andrew D Norden, Hui-Kuo Shu, Patrick Y Wen, and Jeffrey J Olson. Exciting new advances in neuro-oncology: the avenue to a cure for malignant glioma. *CA: a cancer journal for clinicians*, 60(3):166–193, 2010.

18. Elif Ozdemir-Kaynak, Amina A Qutub, and Ozlem Yesil-Celiktas. Advances in glioblastoma multiforme treatment: new models for nanoparticle therapy. *Frontiers in physiology*, 9:170, 2018.

19. P Sapra and TM Allen. Ligand-targeted liposomal anticancer drugs. *Progress in lipid research*, 42(5):439–462, 2003.

20. M Touat, A Idbaih, M Sanson, and KL Ligon. Glioblastoma targeted therapy: updated approaches from recent biological insights. *Annals of Oncology*, 28(7):1457–1472, 2017.

21. I Rubin and Yosef Yarden. The basic biology of her2. *Annals of oncology*, 12:S3–S8, 2001.

22. Sylvie Menard, Serenella Marja Pupa, Manuela Campiglio, and Elda Tagliabue. Biologic and therapeutic role of her2 in cancer. *Oncogene*, 22(42):6570–6578, 2003.

23. Beáta Biri-Kovács, Afrodité Adorján, Ildikó Szabó, Bálint Szeder, Szilvia Bősze, and Gábor Mező. Structure–activity relationship of her2 receptor targeting peptide and its derivatives in targeted tumor therapy. *Biomolecules*, 10(2):183, 2020.

24. Serena Mazzucchelli, Marta Truffi, Luisa Fiandra, Luca Sorrentino, and Fabio Corsi. Targeted approaches for her2 breast cancer therapy: news from nanomedicine? *World Journal of Pharmacology*, 3(4):72–85, 2014.

25. Yasutaka Sukawa, Hiroyuki Yamamoto, Katsuhiko Nosho, Miki Ito, Hisayoshi Igarashi, Takafumi Naito, Kei Mitsuhashi, Yasutaka Matsunaga, Taiga Takahashi, Masashi Mikami, et al. Her2 expression and pi3k-akt pathway alterations in gastric cancer. *Digestion*, 89(1):12–17, 2014.

26. Miriam Colombo, Fabio Corsi, Diego Foschi, Elisa Mazzantini, Serena Mazzucchelli, Carlo Morasso, Emanuela Occhipinti, Laura Polito, Davide Prosperi, Silvia Ronchi, et al. Her2 targeting as a two-sided strategy for breast cancer diagnosis and treatment: Outlook and recent implications in nanomedical approaches. *Pharmacological research*, 62(2):150–165, 2010.

27. Nida Iqbal and Naveed Iqbal. Human epidermal growth factor receptor 2 (her2) in cancers: overexpression and therapeutic implications. *Molecular biology international*, 2014, 2014.

28. Thuy Vu and Francois X Claret. Trastuzumab: updated mechanisms of action and resistance in breast cancer. *Frontiers in oncology*, 2:62, 2012.

29. Gentao Liu, Han Ying, Gang Zeng, Christopher J Wheeler, Keith L Black, and John S Yu. Her-2, gp100, and mage-1 are expressed in human glioblastoma and recognized by cytotoxic t cells. *Cancer research*, 64(14):4980–4986, 2004.

30. Nabil Ahmed, Vita S Salsman, Yvonne Kew, Donald Shaffer, Suzanne Powell, Yi J Zhang, Robert G Grossman, Helen E Heslop, and Stephen Gottschalk. Her2-specific t cells target primary glioblastoma stem cells and induce regression of autologous experimental tumorstargeting stem cells in glioblastoma. *Clinical cancer research*, 16(2):474–485, 2010.

31. Ulrika Andersson, Dongsheng Guo, Beatrice Malmer, A Tommy Bergenheim, Thomas Brännström, Håkan Hedman, and Roger Henriksson. Epidermal growth factor receptor family (egfr, erbb2–4) in gliomas and meningiomas. *Acta neuropathologica*, 108:135–142, 2004.

32. Michael F Press, Carlos Cordon-Cardo, and Dennis J Slamon. Expression of the her-2/neu proto-oncogene in normal human adult and fetal tissues. *Oncogene*, 5(7):953–962, 1990.

33. Coby B Carlson, Patricia Mowery, Robert M Owen, Emily C Dykhuizen, and Laura L Kiessling. Selective tumor cell targeting using low-affinity, multivalent interactions. *ACS chemical biology*, 2(2):119–127, 2007.

34. Pavel I Kitov and David R Bundle. On the nature of the multivalency effect: a thermodynamic model. *Journal of the American Chemical Society*, 125(52):16271–16284, 2003.

35. Xiaohe Tian, Stefano Angioletti-Uberti, and Giuseppe Battaglia. On the design of precision nanomedicines. *Science Advances*, 6(4):eaat0919, 2020.

36. Meng Liu, Azzurra Apriceno, Miguel Sipin, Edoardo Scarpa, Laura Rodriguez-Arco, Alessandro Poma, Gabriele Marchello, Giuseppe Battaglia, and Stefano Angioletti-Uberti. Combinatorial entropy behaviour leads to range selective binding in ligand-receptor interactions. *Nature communications*, 11(1):4836, 2020.

37. Dennis E Discher and Fariyal Ahmed. Polymersomes. *Annu. Rev. Biomed. Eng.*, 8:323–341, 2006.

38. Xiao-ying Zhang and Pei-ying Zhang. Polymersomes in nanomedicine-a review. *Current Nanoscience*, 13(2):124–129, 2017.

39. Alessandro Poma, Yiwen Pei, Lorena Ruiz-Perez, Loris Rizzello, and Giuseppe Battaglia. Polymersomes: Synthesis and applications. *Encyclopedia of Polymer Science and Technology*, pages 1–43, 2002.

40. Anisha A D'souza and Ranjita Shegokar. Polyethylene glycol (peg): a versatile polymer for pharmaceutical applications. *Expert opinion on drug delivery*, 13(9):1257–1275, 2016.

41. Ren Zhong Xiao, Zhao Wu Zeng, Guang Lin Zhou, Jun Jie Wang, Fan Zhu Li, and An Ming Wang. Recent advances in peg–pla block copolymer nanoparticles. *International journal of nanomedicine*, pages 1057–1065, 2010.

42. Giuseppe Battaglia. Polymersomes functionalised with multiple ligands, March 31 2022. US Patent App. 17/419,937.

43. Steven A Cohen and Dennis P Michaud. Synthesis of a fluorescent derivatizing reagent, 6-aminoquinolyl-n-hydroxysuccinimidyl carbamate, and its application for the analysis of hydrolysate amino acids via high-performance liquid chromatography. *Analytical biochemistry*, 211(2):279–287, 1993.

44. Hashem Sharghi, Sakineh Ebrahimpourmoghaddam, Mohammad Mahdi Doroodmand, and Azar Purkhosrow. Synthesis of vasorelaxaing 1, 4-disubstituted 1, 2, 3-triazoles catalyzed by a 4-phenyl-2, 2: 6, 2-terpyridine copper (ii) complex immobilized on activated multiwalled carbon nanotubes. *Asian Journal of Organic Chemistry*, 1(4):377–388, 2012.

45. Jessica Y Shu, Brian Panganiban, and Ting Xu. Peptide-polymer conjugates: from fundamental science to application. *Annual review of physical chemistry*, 64:631–657, 2013.

46. Benjamin Le Droumaguet and Julien Nicolas. Recent advances in the design of bioconjugates from controlled/living radical polymerization. *Polymer Chemistry*, 1(5):563–598, 2010.

47. Hans G Börner. Strategies exploiting functions and self-assembly properties of bioconjugates for polymer and materials sciences. *Progress in Polymer Science*, 34(9):811–851, 2009.

48. James D Robertson, Loris Rizzello, Milagros Avila-Olias, Jens Gaitzsch, Claudia Contini, Monika S Magoń, Stephen A Renshaw, and Giuseppe Battaglia. Purification of nanoparticles by size and shape. *Scientific reports*, 6(1):1–9, 2016.

49. ATCC. Sk-br-3, 2022. Available on line.

50. Ian M Zitron, Archana Thakur, Oxana Norkina, Geoffrey R Barger, Lawrence G Lum, and Sandeep Mittal. Targeting and killing of glioblastoma with activated t cells armed with bispecific antibodies. *BMC cancer*, 13:1–14, 2013.

51. Paola Ringhieri, Silvia Mannucci, Giamaica Conti, Elena Nicolato, Giulio Fracasso, Pasquina Marzola, Giancarlo Morelli, and Antonella Accardo. Liposomes derivatized with multimeric copies of kccysl peptide as targeting agents for her-2-overexpressing tumor cells. *International journal of nanomedicine*, 12:501, 2017.

52. Senthil R Kumar, Fabio A Gallazzi, Riccardo Ferdani, Carolyn J Anderson, Thomas P Quinn, and Susan L Deutscher. In vitro and in vivo evaluation of 64cu-radiolabeled kccysl peptides for targeting epidermal growth factor receptor-2 in breast carcinomas. *Cancer biotherapy & radiopharmaceuticals*, 25(6):693–703, 2010.

53. M Tobıo, A Sanchez, A Vila, I Soriano, C Evora, JL Vila-Jato, and MJ Alonso. The role of peg on the stability in digestive fluids and in vivo fate of peg-pla nanoparticles following oral administration. *Colloids and Surfaces B: Biointerfaces*, 18(3-4):315–323, 2000.

54. Emeline Rideau, Rumiana Dimova, Petra Schwille, Frederik R Wurm, and Katharina Landfester. Liposomes and polymersomes: a comparative review towards cell mimicking. *Chemical society reviews*, 47(23):8572–8610, 2018.

55. Gong-Yan Liu, Chao-Jian Chen, and Jian Ji. Biocompatible and biodegradable polymersomes as delivery vehicles in biomedical applications. *Soft Matter*, 8(34):8811–8821, 2012.